Drivers of plant nutrient acquisition and allocation strategies and their influence on plant responses to environmental change

by

Evan A. Perkowski, B.S.

A Dissertation

In

Biological Sciences

Submitted to the Graduate Faculty
of Texas Tech University in
Partial Fulfillment of
the Requirements for
the Degree of

Doctor of Philosophy

Approved

Dr. Nicholas G. Smith
Chair of Committee

Dr. Aimée T. Classen

Dr. Natasja van Gestel

Dr. Lindsey C. Slaughter

Dr. Dylan W. Schwilk

Dr. Mark Sheridan
Dean of the Graduate School

May 2023

Acknowledgements

Placeholder for text

Table of Contents

Abstract

List of Tables

List of Figures

1 Chapter 1

2 Introduction

Chapter 2

Structural carbon costs to acquire nitrogen are determined by nitrogen and light availability in two species with different nitrogen acquisition strategies

2.1 Introduction

Carbon and nitrogen cycles are tightly coupled in terrestrial ecosystems. This tight coupling influences photosynthesis (Walker et al. 2014; Rogers et al. 2017), net primary productivity (LeBauer and Treseder 2008; Thomas et al. 2013), decomposition (Cornwell et al. 2008; Bonan et al. 2013; Sulman et al. 2019), and plant resource competition (Gill and Finzi 2016; Xu-Ri and Prentice 2017). Terrestrial biosphere models are beginning to include connected carbon and nitrogen cycles to improve the realism of their simulations (Fisher et al. 2010; Brzostek et al. 2014; Wieder et al. 2015; Shi et al. 2016; Zhu et al. 2019). Simulations from these models indicate that coupling carbon and nitrogen cycles can drastically influence future biosphere-atmosphere feedbacks under global change, such as elevated carbon dioxide or nitrogen deposition (Thornton et al. 2007; Goll et al. 2012; Wieder et al. 2015; Wieder et al. 2019). Nonetheless, there are still limitations in our quantitative understanding of connected carbon and nitrogen dynamics (Thomas et al. 2015; Meyerholt et al. 2016; Rogers et al. 2017; Exbrayat et al. 2018; Shi et al. 2019), forcing models to make potentially unreliable assumptions.

Plant nitrogen acquisition is a process in terrestrial ecosystems by which carbon and nitrogen are tightly coupled (Vitousek and Howarth 1991; Delaire et al. 2005; Brzostek et al. 2014). Plants must allocate photosynthetically de-

rived carbon belowground to produce and maintain root systems or exchange with symbiotic soil microbes in order to acquire nitrogen (Högberg et al. 2008; Högberg et al. 2010). Thus, plants have an inherent carbon cost associated with acquiring nitrogen, which can include both direct energetic costs associated with nitrogen acquisition and indirect costs associated with building structures that support nitrogen acquisition (Gutschick 1981; Rastetter et al. 2001; Vitousek et al. 2002; Menge et al. 2008). Model simulations (Fisher et al. 2010; Brzostek et al. 2014; Shi et al. 2016; Allen et al. 2020) and meta-analyses (Terrer et al. 2018) suggest that these carbon costs vary between species, particularly those with different nitrogen acquisition strategies. For example, simulations using iterations of the Fixation and Uptake of Nitrogen (FUN) model indicate that species that acquire nitrogen from non-symbiotic active uptake pathways (e.g. mass flow) generally have larger carbon costs to acquire nitrogen than species that acquire nitrogen through symbiotic associations with nitrogen-fixing bacteria (Brzostek et al. 2014; Allen et al. 2020).

Carbon costs to acquire nitrogen likely vary in response to changes in soil nitrogen availability. For example, if the primary mode of nitrogen acquisition is through non-symbiotic active uptake, then nitrogen availability could decrease carbon costs to acquire nitrogen as a result of increased per-root nitrogen uptake (Franklin et al. 2009; Wang et al. 2018). However, if the primary mode of nitrogen acquisition is through symbiotic active uptake, then nitrogen availability may incur additional carbon costs to acquire nitrogen if it causes microbial symbionts to shift toward parasitism along the parasitism–mutualism continuum (Johnson et al. 1997; Hoek et al. 2016; Friel and Friesen 2019) or if it reduces

the nitrogen acquisition capacity of a microbial symbiont (van Diepen et al. 2007; Soudzilovskaia et al. 2015; Muñoz et al. 2016). Species may respond to shifts in soil nitrogen availability by switching their primary mode of nitrogen acquisition to a strategy with lower carbon costs to acquire nitrogen in order to maximize the magnitude of nitrogen acquired from a belowground carbon investment and outcompete other individuals for soil resources (Rastetter et al. 2001; Menge et al. 2008).

Environmental conditions that affect demand to acquire nitrogen to support new and existing tissues could also be a source of variance in plant carbon costs to acquire nitrogen. For example, an increase in plant nitrogen demand could increase carbon costs to acquire nitrogen if this increases the carbon that must be allocated belowground to acquire a proportional amount of nitrogen (Kulmatiski et al. 2017; Noyce et al. 2019). This could be driven by a temporary state of diminishing return associated with investing carbon toward building and maintaining structures that are necessary to support enhanced nitrogen uptake, such as fine roots (Matamala and Schlesinger 2000; Norby et al. 2004; Arndal et al. 2018), mycorrhizal hyphae (Saleh et al. 2020), or root nodules (Parvin et al. 2020). Alternatively, if the environmental factor that increases plant nitrogen demand causes nitrogen to become more limiting in the system (e.g. atmospheric CO2; Luo et al. (2004), LeBauer and Treseder (2008), Vitousek et al. (2010), Liang et al. (2016)), species might switch their primary mode of nitrogen acquisition to a strategy with lower relative carbon costs to acquire nitrogen in order to gain a competitive advantage over species with either different or more limited modes of nitrogen acquisition (Ainsworth and Long 2005; Taylor and Menge 2018).

Using a plant economics approach, we examined the influence of plant nitrogen demand and soil nitrogen availability on plant carbon costs to acquire nitrogen. This was done by growing a species capable of forming associations with nitrogen-fixing bacteria (*Glycine max* L. (Merr)) and a species not capable of forming these associations (*Gossypium hirsutum* L.) under four levels of light availability (plant nitrogen demand proxy) and four levels of soil nitrogen fertilization (soil nitrogen availability proxy) in a full-factorial, controlled greenhouse experiment. We used this experimental set-up to test the following hypotheses:

1. An increase in plant nitrogen demand due to increasing light availability will increase carbon costs to acquire nitrogen through a proportionally larger increase in belowground carbon than whole-plant nitrogen acquisition. This will be the result of an increased investment of carbon toward belowground structures that support enhanced nitrogen uptake, but at a lower nitrogen return.

2. An increase in soil nitrogen availability will decrease carbon costs to acquire nitrogen as a result of increased per root nitrogen uptake in *G. hirsutum*. However, soil nitrogen availability will not affect carbon costs to acquire nitrogen in *G. max* because of the already high return of nitrogen supplied through nitrogen fixation.

2.2 Methods

2.2.1 *Experiment setup*

Gossypium hirsutum and *G. max* were planted in individual 3 liter pots (NS-300; Nursery Supplies, Orange, CA, USA) containing a 3:1 mix of unfertilized potting mix (Sungro Sunshine Mix #2, Agawam, MA, USA) to native soil extracted from an agricultural field most recently planted with *G. max* at the USDA-ARS Laboratory in Lubbock, TX, USA (33.59°N, –101.90°W). The field soil was classified as Amarillo fine sandy loam (75% sand, 10% silt, 15% clay). Upon planting, all *G. max* pots were inoculated with *Bradyrhizobium japonicum* (Verdesian N-Dure™ Soybean, Cary, NC, USA) to stimulate root nodulation. Individuals of both species were grown under similar, unshaded, ambient greenhouse conditions for 2 weeks to germinate and begin vegetative growth. Three blocks were set up in the greenhouse, each containing four light treatments created using shade cloth that reduced incoming radiation by either 0 (full sun), 30, 50, or 80%. Two weeks post-germination, individuals were randomly placed in the four light treatments in each block. Individuals received one of four nitrogen fertilization doses as 100ml of a modified Hoagland solution (Hoagland and Arnon 1950) equivalent to either 0, 70, 210, or 630 ppm N twice per week within each light treatment. Nitrogen fertilization doses were received as topical agents to the soil surface. Each Hoagland solution was modified to keep concentrations of other macro- and micronutrients equivalent (Supplementary Table S1). Plants were routinely well watered to eliminate water stress.

2.2.2 *Plant measurements and calculations*

Each individual was harvested after 5 weeks of treatment, and biomass was separated by organ type (leaves, stems, and roots). Nodules on *G. max* roots were also harvested. With the exception of the 0% shade cover and 630 ppm N treatment combination, all treatment combinations in both species had lower average dry biomass:pot volume ratios than the 1:1 ratio recommended by Poorter et al. (2012) to minimize the likelihood of pot volume-induced growth limitation (Supplementary Tables S2, S3; Supplementary Fig. S1). All harvested material was dried, weighed, and ground by organ type. Carbon and nitrogen content (g g^{-1}) was determined by subsampling from ground and homogenized biomass of each organ type using an elemental analyzer (Costech 4010; Costech, Inc., Valencia, CA, USA). We scaled these values to total leaf, stem, and root carbon and nitrogen biomass (g) by multiplying dry biomass of each organ type by carbon or nitrogen content of each corresponding organ type. Whole-plant nitrogen biomass (g) was calculated as the sum of total leaf (g), stem (g), and root (g) nitrogen biomass. Root nodule carbon biomass was not included in the calculation of root carbon biomass; however, relative plant investment toward root or root nodule standing stock was estimated as the ratio of root biomass to root nodule biomass (g g^{-1}), following similar metrics to those adopted by Dovrat et al. (2018) and Dovrat et al. (2020).

Carbon costs to acquire nitrogen (gC gN^{-1}) were estimated as the ratio of total root carbon biomass (gC) to whole-plant nitrogen biomass (gN). This calculation quantifies the relationship between carbon spent on nitrogen acquisition and whole-plant nitrogen acquisition by using root carbon biomass as a proxy for

estimating the magnitude of carbon allocated toward nitrogen acquisition. This calculation therefore assumes that the magnitude of root carbon standing stock is proportional to carbon transferred to root nodules or mycorrhizae, or lost through root exudation or turnover. This assumption has been supported in species that associate with ectomycorrhizal fungi (Hobbie 2006; Hobbie and Hobbie 2008), but is less clear in species that acquire nitrogen through non-symbiotic active uptake or symbiotic nitrogen fixation. It is also unclear whether relationships between root carbon standing stock and carbon transfer to root nodules are similar in magnitude to carbon lost through exudation or when allocated toward other active uptake pathways. Thus, because of the way we performed our measurements, our proximal values of carbon costs to acquire nitrogen are underestimates.

2.2.3 *Statistical analyses*

We explored the effects of light and nitrogen availability on carbon costs to acquire nitrogen using separate linear mixed-effects models for each species. Models included shade cover, nitrogen fertilization, and interactions between shade cover and nitrogen fertilization as continuous fixed effects, and also included block as a random intercept term. Three separate models for each species were built with this independent variable structure for three different dependent variables: (i) carbon costs to acquire nitrogen (gC gN^{-1}); (ii) whole-plant nitrogen biomass (denominator of carbon cost to acquire nitrogen; gN); and (iii) root carbon biomass (numerator of carbon cost to acquire nitrogen; gC). We constructed two additional models for *G. max* with the same model structure described above to investigate the effects of light availability and nitrogen fertilization on root nodule biomass

(g) and the ratio of root nodule biomass to root biomass (unitless).

We used Shapiro–Wilk tests of normality to determine whether species-specifc linear mixed-effects model residuals followed a normal distribution. None of our models satisfied residual normality assumptions when models were fit using untransformed data (Shapiro–Wilk: $P<0.05$ in all cases). We attempted to satisfy residual normality assumptions by first fitting models using dependent variables that were natural-log transformed. If residual normality assumptions were still not met (Shapiro–Wilk: $P<0.05$), then models were fit using dependent variables that were square root transformed. All residual normality assumptions were satisfied when models were fit with either a natural-log or square root transformation (Shapiro–Wilk: $P>0.05$ in all cases). Specifically, we natural-log transformed *G. hirsutum* carbon costs to acquire nitrogen and *G. hirsutum* whole-plant nitrogen biomass. We also square root transformed *G. max* carbon costs to acquire nitrogen, *G. max* whole-plant nitrogen biomass, root carbon biomass in both species, *G. max* root nodule biomass, and the *G. max* ratio of root nodule biomass to root biomass. We used the 'lmer' function in the 'lme4' R package (Bates et al. 2015) to fit each model and the 'Anova' function in the 'car' R package (Fox and Weisberg 2019) to calculate Wald's χ^2 to determine the significance (α=0.05) of each fixed effect coefficient. Finally, we used the 'emmeans' R package (Lenth 2019) to conduct post-hoc comparisons of our treatment combinations using Tukey's tests. Degrees of freedom for all Tukey's tests were approximated using the Kenward–Roger approach (Kenward and Roger 1997). All analyses and plots were conducted in R version 4.0.1 (R Core Team 2021).

2.3 Results

2.3.1 *Carbon costs to acquire nitrogen*

Carbon costs to acquire nitrogen in *G. hirsutum* increased with increasing light availability (P<0.001; Table 1; Fig. 1) and decreased with increasing nitrogen fertilization (P<0.001; Table 1; Fig. 1). There was no interaction between light availability and nitrogen fertilization (P=0.486; Table 2.1; Fig. 2.1).

Carbon costs to acquire nitrogen in *G. max* also increased with increasing light availability (P<0.001; Table 1; Fig. 1) and decreased with increasing nitrogen fertilization (P<0.001; Table 1; Fig. 1). There was no interaction between light availability and nitrogen fertilization (P=0.261; Table 2.1; Fig. 2.1).

Table 2.1. Analysis of variance results exploring species-specific effects of light availability, nitrogen fertilization, and their interactions on carbon costs to acquire nitrogen, whole-plant nitrogen biomass, and root carbon biomass

		Carbon costs to acquire nitrogen			Whole-plant nitrogen biomass			Root carbon biomass		
	df	Coefficient	χ^2	*P*-value	Coefficient	χ^2	*P*-value	Coefficient	χ^2	*P*-value
G. hirsutum										
Intercept		1.594	-	-	-3.232	-	-	0.432	-	-
Light (L)	1	-1.09E-02	56.494	**<0.001**	-6.41E-03	91.275	**<0.001**	-2.62E-03	169.608	**<0.001**
Nitrogen (N)	1	-1.34E-03	54.925	**<0.001**	1.83E-03	118.784	**<0.001**	1.15E-04	2.901	*0.089*
L*N	1	3.88E-06	0.485	0.486	-1.34E-05	10.721	**0.001**	-1.67E-06	3.140	*0.076*
G. max										
Intercept		1.877	-	-	0.239	-	-	0.438	-	-
Light (L)	1	-7.67E-03	174.156	**<0.001**	-6.72E-04	39.799	**<0.001**	-2.55E-03	194.548	**<0.001**
Nitrogen (N)	1	-2.35E-04	21.948	**<0.001**	1.55E-04	70.771	**<0.001**	2.52E-04	19.458	**<0.001**
L*N	1	-2.89E-06	1.262	0.261	-6.32E-07	1.435	0.231	-3.16E-06	10.803	**0.001**

*Significance determined using Wald's χ^2 tests (P=0.05). P-values<0.05 are in bold and marginally insignificant P-values between 0.050 and 0.100 are italicized. Negative coefficients for light treatments indicate a positive effect of increasing light availability on all response variables, as light availability is treated as percent shade cover in all linear mixed-effects models.

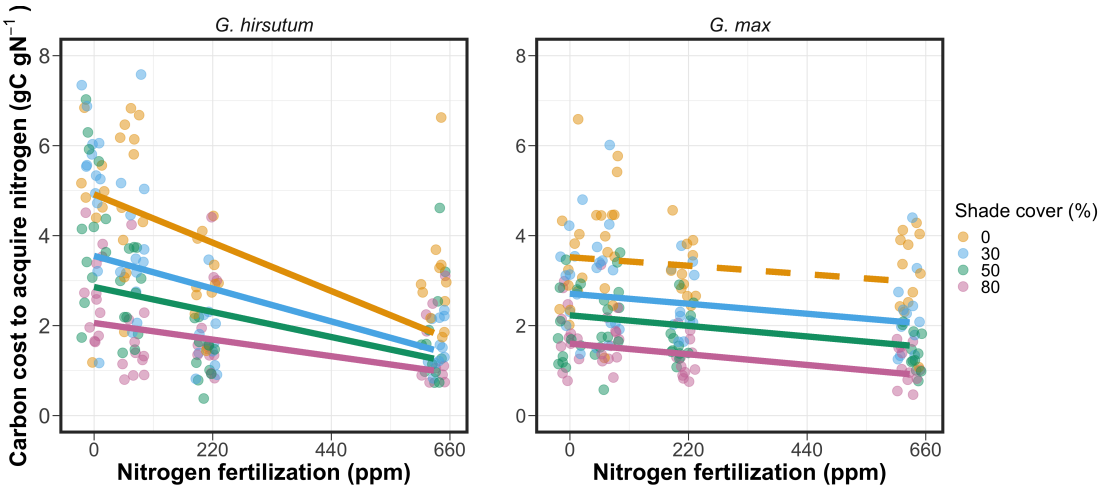

Figure 2.1. Relationships between soil nutrient fertilization and light availability on carbon costs to acquire nitrogen in *G. hirsutum* and *G. max*. Nitrogen fertilization treatments are represented on the x-axis. Shade cover treatments are represented through colored points and trendlines. Trendlines were created by back-transforming marginal mean slopes and intercepts from species-specific linear mixed-effects models. These values were calculated using the 'emtrends' and 'emmeans' functions in the 'emmeans' R package (Lenth, 2019). Points are jittered for visibility. Yellow points and trendlines represent the 0% shade cover treatment, blue points and trendlines represent the 30% shade cover treatment, green points and trendlines represent the 50% shade cover treatment, and purple points and trendlines represent the 80% shade cover treatment. Solid trendlines indicate slopes that are significantly different from zero (Tukey: $P<0.05$), while dashed trendlines indicate slopes that are not statistically different from zero.

2.3.2 *Whole plant nitrogen biomass*

Whole-plant nitrogen biomass in *G. hirsutum* was driven by an interaction between light availability and nitrogen fertilization (P=0.001; Table 1; Fig. 2). This interaction indicated a greater stimulation of whole-plant nitrogen biomass by nitrogen fertilization as light levels increased (Table 2.1; Fig. 2.2).

Whole-plant nitrogen biomass in *G. max* increased with increasing light availability (P<0.001) and nitrogen fertilization (P<0.001), with no interaction between light availability and nitrogen fertilization (P=0.231; Table 2.1; Fig. 2.2).

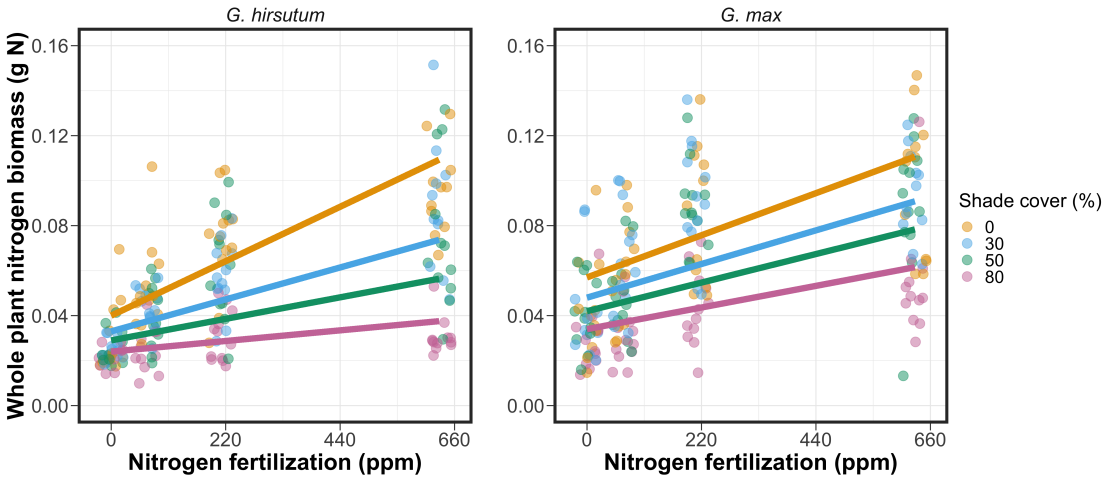

Figure 2.2. Relationships between soil nutrient fertilization and light availability on whole-plant nitrogen biomass in *G. hirsutum* and *G. max*.Whole-plant nitrogen biomass is the denominator of the carbon cost to acquire nitrogen calculation. Nitrogen fertilization treatments are represented on the x-axis. Shade cover treatments are represented through colored points and trendlines. Trendlines were created by back-transforming marginal mean slopes and intercepts from species-specific linear mixed-effects models. These values were calculated using the 'emtrends' and 'emmeans' functions in the 'emmeans' R package (Lenth 2019). Points are jittered for visibility. Yellow points and trendlines represent the 0% shade cover treatment, blue points and trendlines represent the 30% shade cover treatment, green points and trendlines represent the 50% shade cover treatment, and purple points and trendlines represent the 80% shade cover treatment. Solid trendlines indicate slopes that are significantly different from zero (Tukey: $P<0.05$), while dashed trendlines indicate slopes that are not statistically different from zero.

2.3.3 *Root carbon biomass*

Root carbon biomass in *G. hirsutum* significantly increased with increasing light availability (P<0.001; Table 1; Fig. 3) and marginally increased with nitrogen fertilization (P=0.089; Table 1; Fig. 3). There was also a marginal interaction between light availability and nitrogen fertilization (P=0.076; Table 1), driven by an increase in the positive response of root carbon biomass to increasing nitrogen fertilization as light availability increased. This resulted in significantly positive trends between root carbon biomass and nitrogen fertilization in the two highest light treatments (Tukey: P<0.05 in both cases; Table 2.3; Fig. 2.3) and no effect of nitrogen fertilization in the two lowest light treatments (Tukey: P>0.05 in both cases; Table 3; Fig. 3).

There was an interaction between light availability and nitrogen fertilization on root carbon biomass in *G. max* (P=0.001; Table 1; Fig. 3). Post-hoc analyses indicated that the positive effects of nitrogen fertilization on G.! max root carbon biomass increased with increasing light availability (Table 3; Fig. 3). There were also positive individual effects of increasing nitrogen fertilization (P<0.001) and light availability (P<0.001) on *G. max* root carbon biomass (Table 1; Fig. 2.3).

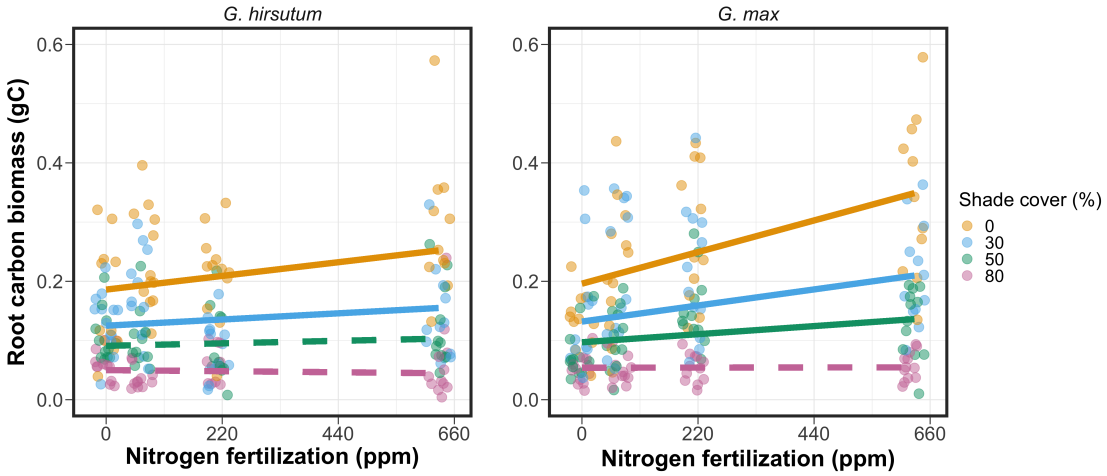

Figure 2.3. Relationships between soil nutrient fertilization and light availability on root carbon biomass in *G. hirsutum* and *G. max*. Root carbon biomass is the numerator of the carbon cost to acquire nitrogen calculation. Nitrogen fertilization treatments are represented on the x-axis. Shade cover treatments are represented through colored points and trendlines. Trendlines were created by back-transforming marginal mean slopes and intercepts from species-specific linear mixed-effects models. These values were calculated using the 'emtrends' and 'emmeans' functions in the 'emmeans' R package (Lenth 2019). Points are jittered for visibility. Yellow points and trendlines represent the 0% shade cover treatment, blue points and trendlines represent the 30% shade cover treatment, green points and trendlines represent the 50% shade cover treatment, and purple points and trendlines represent the 80% shade cover treatment. Solid trendlines indicate slopes that are significantly different from zero (Tukey: $P<0.05$), while dashed trendlines indicate slopes that are not statistically different from zero.

2.3.4 *Root nodule biomass*

Root nodule biomass in *G. max* increased with increasing light availability (P<0.001; Table 2; Fig. 4A) and decreased with increasing nitrogen fertilization (P<0.001; Table 2; Fig. 4A). There was no interaction between nitrogen fertilization and light availability (P=0.133; Table 2; Fig. 4A). The ratio of root nodule biomass to root biomass did not change in response to light availability (P=0.481; Table 2; Fig. 4B) but decreased with increasing nitrogen fertilization (P<0.001; Table 2; Fig. 4B). There was no interaction between nitrogen fertilization and light availability on the ratio of root nodule biomass to root biomass (P=0.621; Table 2; Fig. 4B).

Table 2.2. Analysis of variance results exploring effects of light availability, nitrogen fertilization, and their interactions on *G. max* root nodule biomass and the ratio of root nodule biomass to root biomass*

		Nodule biomass			Nodule biomass: root biomass		
	df	Coefficient	χ^2	*P*-value	Coefficient	χ^2	*P*-value
Intercept		0.302	-	-	0.448	-	-
Light (L)	1	-1.81E-03	72.964	**<0.001**	-8.76E-05	0.496	0.481
Nitrogen (N)	1	-2.83E-04	115.377	**<0.001**	-5.09E-04	156.476	**<0.001**
L*N	1	1.14E-06	2.226	0.133	-7.30E-07	0.244	0.621

*Significance determined using Wald's χ^2 tests (α=0.05). *P*-values less than 0.05 are in bold. Negative coefficients for light treatments indicate a positive effect of increasing light availability on all response variables, as light availability is treated as percent shade cover in all linear mixed-effects models. Root nodule biomass and nodule biomass: root biomass models were only constructed for G. max because *G. hirsutum* was not inoculated with *B. japonicum* and is not capable of forming root nodules.

Table 2.3. Slopes of the regression line describing the relationship between each dependent variable and nitrogen fertilization at each light level*

Shade cover	Carbon cost to acquire nitrogen	Whole-plant nitrogen biomass	Root carbon biomass	Root nodule biomass	Nodule biomass root biomass
G. hirsutum					
0%	**-1.34E-03^{a}**	**1.83E-03^{a}**	**1.15E-04^{b}**	-	-
30%	**-1.22E-03^{a}**	**1.43E-03^{a}**	**1.17E-04^{b}**	-	-
50%	**-1.14E-03^{a}**	**1.17E-03^{a}**	3.12E-05^{b}	-	-
80%	**-1.02E-03^{a}**	**7.66E-04^{a}**	-1.89E-06^{b}	-	-
G. max					
0%	-2.35E-04^{b}	**1.55E-05^{b}**	**2.51E-04^{b}**	**-2.83E-04^{b}**	**-5.09E-04^{b}**
30%	**-3.22E-04^{b}**	**1.35E-05^{b}**	**1.57E-04^{b}**	**-2.49E-04^{b}**	**-5.31E-04^{b}**
50%	**-3.80E-04^{b}**	**1.23E-05^{b}**	**9.37E-05^{b}**	**-2.26E-04^{b}**	**-5.45E-04^{b}**
80%	**-4.66E-04^{b}**	**1.04E-05^{b}**	-9.95E-07^{b}	**-1.92E-04^{b}**	**-5.67E-04^{b}**

*Slopes represent estimated marginal mean slopes from linear mixed-effects models described in the Methods. Slopes were calculated using the 'emmeans' R package (Lenth 2019). Superscripts indicate slopes fit to natural-log (^{a}) or square root (^{b}) transformed data. Slopes statistically different from zero (Tukey: $P<0.05$) are indicated in bold. Marginally significant slopes (Tukey: $0.05<P<0.1$) are italicized.

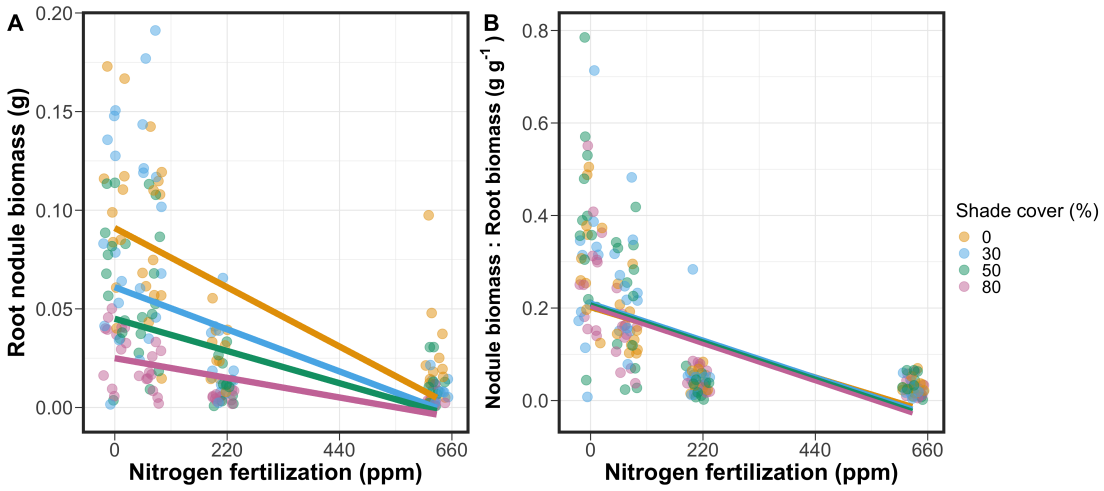

Figure 2.4. Effects of shade cover and nitrogen fertilization on root nodule biomass (A) and the ratio of root nodule biomass to root biomass (B) in *G. max*. Nitrogen fertilization treatments are represented on the x-axis. Shade cover treatments are represented through colored points and trendlines. Trendlines were created by back-transforming marginal mean slopes and intercepts from species-specific linear mixed-effects models. These values were calculated using the 'emtrends' and 'emmeans' functions in the 'emmeans' R package (Lenth, 2019). Points are jittered for visibility. Yellow points and trendlines represent the 0% shade cover treatment, blue points and trendlines represent the 30% shade cover treatment, green points and trendlines represent the 50% shade cover treatment, and purple points and trendlines represent the 80% shade cover treatment. Solid trendlines indicate slopes that are significantly different from zero (Tukey: $P<0.05$), while dashed trendlines indicate slopes that are not statistically different from zero.

2.4 Discussion

In this chapter, we determined the effects of light availability and soil nitrogen fertilization on root mass carbon costs to acquire nitrogen in *G. hirsutum* and *G. max*. In support of our hypotheses, we found that carbon costs to acquire nitrogen generally increased with increasing light availability and decreased with increasing soil nitrogen fertilization in both species. These findings suggest that carbon costs to acquire nitrogen are determined by factors that influence plant nitrogen demand and soil nitrogen availability. In contrast to our second hypothesis, root nodulation data suggested that *G. max* and *G. hirsutum* achieved similar directional carbon cost responses to nitrogen fertilization despite a likely shift in G.!max allocation from nodulation to root biomass along the nitrogen fertilization gradient (Fig. 2.4B).

Both *G. max* and *G. hirsutum* experienced an increase in carbon costs to acquire nitrogen due to increasing light availability. These patterns were driven by a larger increase in root carbon biomass than whole-plant nitrogen biomass. Increases in root carbon biomass due to factors that increase plant nitrogen demand are a commonly observed pattern, as carbon allocated belowground provides substrate needed to produce and maintain structures that satisfy aboveground plant nitrogen demand (Nadelhoffer and Raich 1992; Giardina et al. 2005; Raich et al. 2014). Our findings suggest that plants allocate relatively more carbon for acquiring nitrogen when demand increases over short temporal scales, which may cause a temporary state of diminishing return due to asynchrony between belowground carbon and whole-plant nitrogen responses to plant nitrogen demand (Kulmatiski et al. 2017; Noyce et al. 2019). These responses might be attributed to a temporal

lag associated with producing structures that enhance nitrogen acquisition. For example, fine roots (Matamala and Schlesinger 2000; Norby et al. 2004; Arndal et al. 2018) and root nodules (Parvin et al. 2020) take time to build and first require the construction of coarse roots. Thus, full nitrogen returns from these investments may not occur immediately (Kayler et al. 2010; Kayler et al. 2017), and may vary by species acquisition strategy. We speculate that increases in nitrogen acquisition from a given carbon investment may occur beyond the 5 week scope of this experiment. A similar study conducted over a longer temporal scale would address this.

Increasing soil nitrogen fertilization generally decreased carbon costs to acquire nitrogen in both species. These patterns were driven by a larger increase in whole-plant nitrogen biomass than root carbon biomass. In *G. hirsutum*, reductions in carbon costs to acquire nitrogen may have been due to an increase in per-root nitrogen uptake, allowing individuals to maximize the amount of nitrogen acquired from a belowground carbon investment. Interestingly, increased soil nitrogen fertilization increased whole-plant nitrogen biomass in *G. max* despite reductions in root nodule biomass that likely reduced the nitrogen-fixing capacity of *G. max* (Andersen et al. 2005; Muñoz et al. 2016). While reductions in root nodulation due to increased soil nitrogen availability are commonly observed (Gibson and Harper 1985; Fujikake et al. 2003), our responses were observed in tandem with increased root carbon biomass, implying that *G. max* shifted relative carbon allocation from nitrogen fixation to soil nitrogen acquisition (Markham and Zekveld 2007; Dovrat et al. 2020). This was likely because there was a reduction in the carbon cost advantage of acquiring fixed nitrogen relative to soil nitrogen, and

suggests that species capable of associating with symbiotic nitrogen-fixing bacteria shift their relative nitrogen acquisition pathway to optimize nitrogen uptake (Rastetter et al. 2001). Future studies should further investigate these patterns with a larger quantity of phylogenetically related species, or different varieties of a single species that differ in their ability to form associations with symbiotic nitrogen-fixing bacteria to more directly test the impact of nitrogen fixation on the patterns observed in this study.

Carbon costs to acquire nitrogen are subsumed in the general discussion of economic analogies to plant resource uptake (Bloom et al. 1985; Rastetter et al. 2001; Vitousek et al. 2002; Phillips et al. 2013; Terrer et al. 2018; Henneron et al. 2020). Despite this, terrestrial biosphere models rarely include these carbon costs within their framework for predicting plant nitrogen uptake. There is currently one plant resource uptake model, FUN, that quantitatively predicts carbon costs to acquire nitrogen within a framework for predicting plant nitrogen uptake for different nitrogen acquisition strategies (Fisher et al. 2010; Brzostek et al. 2014)

(Fisher et al. 2010; Brzostek et al. 2014). Iterations of FUN are currently coupled to two terrestrial biosphere models: the Community Land Model 5.0 and the Joint UK Land Environment Simulator (Shi et al. 2016; Lawrence et al. 2019; Clark et al. 2011). Recent work suggests that coupling FUN to CLM 5.0 caused a large overprediction of plant nitrogen uptake associated with nitrogen fixation (Davies-Barnard et al. 2020). Thus, empirical data from manipulative experiments that explicitly quantify carbon costs to acquire nitrogen in species capable of associating with nitrogen-fixing bacteria across different environmental contexts is an important step toward identifying potential biases in models such

as FUN.

Our findings broadly support the FUN formulation of carbon costs to acquire nitrogen in response to soil nitrogen availability. FUN calculates carbon costs to acquire nitrogen based on the sum of carbon costs to acquire nitrogen via nitrogen fixation, mycorrhizal active uptake, non-mycorrhizal active uptake, and retranslocation

(Fisher et al. 2010; Brzostek et al. 2014). Carbon costs to acquire nitrogen via mycorrhizal or non-mycorrhizal active uptake pathways are derived as a function of nitrogen availability, root biomass, and two parameterized values based on nitrogen acquisition strategy (Brzostek et al. 2014). Due to this, FUN simulates a net decrease in carbon costs to acquire nitrogen with increasing nitrogen availability for mycorrhizal and non-mycorrhizal active uptake pathways, assuming constant root biomass. This was a pattern we observed in *G. hirsutum* regardless of light availability. In contrast, FUN would not simulate a net change in carbon costs to acquire nitrogen via nitrogen fixation due to nitrogen availability. This is because carbon costs to acquire nitrogen via nitrogen fixation are derived from a well-established function of soil temperature, which is independent of soil nitrogen availability (Houlton et al. 2008; Fisher et al. 2010). We observed a net reduction in carbon costs to acquire nitrogen in *G. max*, except when individuals were grown under 0% shade cover (Fig. 1). While a net reduction of carbon costs in response to nitrogen fertilization runs counter to nitrogen fixation carbon costs simulated by FUN, these patterns were likely because *G. max* individuals switched their primary mode of nitrogen acquisition from symbiotic nitrogen fixation to a non-symbiotic active uptake pathway (Fig. 4B).

328 It should be noted that the metric used in this study to determine carbon
329 costs to acquire nitrogen has several limitations. Most notably, this metric uses
330 root carbon biomass as a proxy for estimating the amount of carbon spent on
331 nitrogen acquisition. While it is true that most carbon allocated belowground
332 has at least an indirect structural role in acquiring soil resources, it remains un-
333 clear whether this assumption holds true for species that acquire nitrogen via
334 symbiotic nitrogen fixation. We also cannot quantify carbon lost through root
335 exudates or root turnover, which may increase due to factors that increase plant
336 nitrogen demand (Tingey et al. 2000; Phillips et al. 2011), and can increase the
337 magnitude of available nitrogen from soil organic matter through priming effects
338 on soil microbial communities (Uselman et al. 2000; Bengtson et al. 2012). It
339 is also not clear whether these assumptions hold under all environmental condi-
340 tions, such as those that shift belowground carbon allocation toward a different
341 mode of nitrogen acquisition (Taylor and Menge 2018; Friel and Friesen 2019)
342 or between species with different acquisition strategies. In this study, increasing
343 soil nitrogen fertilization increased carbon investment to roots relative to carbon
344 transferred to root nodules (Fig. 4B). By assuming that carbon allocated to root
345 carbon was proportional to carbon allocated to root nodules across all treatment
346 combinations, these observed responses to soil nitrogen fertilization were likely
347 to be overestimated in *G. max*. We encourage future research to quantify these
348 carbon fates independently.

349 Researchers conducting pot experiments must carefully choose pot volume
350 to minimize the likelihood of pot volume-induced growth limitation (Poorter et al.
351 2012). Poorter et al. (2012) indicate that researchers are likely to avoid growth

limitations associated with pot volume if measurements are collected when the plant biomass:pot volume ratio is less than 1 g L^{-1}. In this experiment, all treatment combinations in both species had biomass:pot volume ratios less than 1 g L^{-1} except for *G. max* and *G. hirsutum* that were grown under 0% shade cover and had received 630 ppm N. Specifically, *G. max* and *G. hirsutum* had average respective biomass:pot volume ratios of 1.24±0.07g L^{-1} and 1.34±0.13 g L^{-1}, when grown under 0% shade cover and received 630 ppm N (Supplementary Tables S2, S3; Supplementary Fig. S1). If growth in this treatment combination was limited by pot volume, then individuals may have had larger carbon costs to acquire nitrogen than would be expected if they were grown in larger pots. This pot volume induced growth limitation could cause a reduction in per-root nitrogen uptake associated with more densely packed roots, which could reduce the positive effect of nitrogen fertilization on whole-plant nitrogen biomass relative to root carbon biomass (Poorter et al. 2012).

Growth limitation associated with pot volume provides a possible explanation for the marginally insignificant effect of increasing nitrogen fertilization on *G. max* carbon costs to acquire nitrogen when grown under 0% shade cover (Table 3; Fig. 1). This is because the regression line describing the relationship between carbon costs to acquire nitrogen and nitrogen fertilization in *G. max* grown under 0% shade cover would have flattened if growth limitation had caused larger than expected carbon costs to acquire nitrogen in the 0% shade cover, 630 ppm N treatment combination. This may have been exacerbated by the fact that *G. max* likely shifted relative carbon allocation from nitrogen fixation to soil nitrogen acquisition, which could have increased the negative effect of more densely packed

roots on nitrogen uptake. These patterns could have also occurred in *G. hirsutum* grown under 0% shade cover; however, there was no change in the effect of nitrogen fertilization on *G. hirsutum* carbon costs to acquire nitrogen grown under 0% shade cover relative to other shade cover treatments. Regardless, the possibility of growth limitation due to pot volume suggests that effects of increasing nitrogen fertilization on carbon costs to acquire nitrogen in both species grown under 0% shade cover could have been underestimated. Follow-up studies using a similar experimental design with a larger pot volume would be necessary in order to determine whether these patterns were impacted by pot volume-induced growth limitation.

In conclusion, this study provides empirical evidence that carbon costs to acquire nitrogen are influenced by light availability and soil nitrogen fertilization in a species capable of acquiring nitrogen via symbiotic nitrogen fixation and a species not capable of forming such associations. We show that carbon costs to acquire nitrogen generally increase with increasing light availability and decrease with increasing nitrogen fertilization. This study provides important empirical data needed to evaluate the formulation of carbon costs to acquire nitrogen in terrestrial biosphere models, particularly carbon costs to acquire nitrogen that are associated with symbiotic nitrogen fixation. Our findings broadly support the general formulation of these carbon costs in the FUN biogeochemical model in response to shifts in nitrogen availability. However, there is a need for future studies to explicitly quantify carbon costs to acquire nitrogen under different environmental contexts, over longer temporal scales, and using larger selections of phylogenetically related species. In addition, we suggest that future studies mini-

mize the limitations associated with the metric used here by explicitly measuring belowground carbon fates independently.

Chapter 3

Soil nitrogen availability modifies leaf nitrogen economies in mature temperate deciduous forests: a direct test of photosynthetic least-cost theory

3.1 Introduction

Photosynthesis represents the largest carbon flux between the atmosphere and land surface (IPCC 2021), and plays a central role in biogeochemical cycling at multiple spatial and temporal scales (Vitousek and Howarth 1991; LeBauer and Treseder 2008; Kaiser et al. 2015; Wieder et al. 2015). Therefore, carbon and energy fluxes simulated by terrestrial biosphere models are sensitive to the formulation of photosynthetic processes (Ziehn et al. 2011; Bonan et al. 2011; Booth et al. 2012; Smith et al. 2016; Smith et al. 2017) and must be represented using robust, empirically tested processes (Prentice et al. 2015; Wieder et al. 2019). Current formulations of photosynthesis vary across terrestrial biosphere models (Smith and Dukes 2013; Rogers et al. 2017), which causes variation in modeled ecosystem processes (Knorr 2000; Knorr and Heimann 2001; Bonan et al. 2011; Friedlingstein et al. 2014) and casts uncertainty on the ability of these models to accurately predict terrestrial ecosystem responses and feedbacks to global change (Zaehle et al. 2005; Schaefer et al. 2012; Davies-Barnard et al. 2020).

Terrestrial biosphere models commonly represent C_3 photosynthesis through variants of the Farquhar et al. (1980) biochemical model (Smith and Dukes 2013; Rogers 2014; Rogers et al. 2017). This well-tested photosynthesis model estimates leaf-level carbon assimilation, or photosynthetic capacity, as a function of the maximum rate of Ribulose-1,5-bisphosphate carboxylase-oxygenase (Ru-

bisco) carboxylation (V_{cmax}) and the maximum rate of Ribulose-1,5-bisphosphate (RuBP) regeneration (J_{max}) (Farquhar et al. 1980). Many terrestrial biosphere models predict these model inputs based on plant functional group specific linear relationships between leaf nutrient content and V_{cmax} (Smith and Dukes 2013; Rogers 2014; Rogers et al. 2017) under the tenet that a large fraction of leaf nutrients, and nitrogen (N) in particular, are partitioned toward building and maintaining enzymes that support photosynthetic capacity, such as Rubisco (Brix 1971; Gulmon and Chu 1981; Evans 1989; Kattge et al. 2009; Walker et al. 2014). Terrestrial biosphere models also predict leaf nutrient content from soil nutrient availability based on the assumption that increasing soil nutrients generally increases leaf nutrients (Firn et al. 2019; Li et al. 2020; Liang et al. 2020) which, in the case of N, generally corresponds with an increase in photosynthetic processes (Li et al. 2020; Liang et al. 2020).

Recent work calls the generality of relationships between soil nutrient availability, leaf nutrient content, and photosynthetic capacity into question, suggesting instead that leaf nutrients and photosynthetic capacity are better predicted as an integrated product of aboveground climate, leaf traits, and soil nutrient availability, rather than soil nutrient availability alone (Dong et al. 2017; Dong et al. 2020; Dong et al. 2022; Firn et al. 2019; Smith et al. 2019; Peng et al. 2021). It has been reasoned that this result is because plants allocate added nutrients to growth and storage rather than alterations in leaf chemistry (Smith et al. 2019), perhaps as a result of nutrient limitation of primary productivity (LeBauer and Treseder 2008; Fay et al. 2015). Additionally, recent work suggests that relationships between leaf nutrient content and photosynthesis vary across environments,

and that the proportion of leaf nutrient content allocated to photosynthetic tissue varies over space and time with plant acclimation and adaptation responses to light availability, vapor pressure deficit, soil pH, soil nutrient availability, and environmental factors that influence leaf mass per area (Pons and Pearcy 1994; Niinemets and Tenhunen 1997; Evans and Poorter 2001; Hikosaka and Shigeno 2009; Ghimire et al. 2017; Onoda et al. 2017; Luo et al. 2021). The use of linear relationships between leaf nutrient content and Vcmax to predict photosynthetic capacity, as commonly used in terrestrial biosphere models (Rogers 2014), is not capable of detecting such responses.

Photosynthetic least-cost theory provides an alternative framework for understanding relationships between soil nutrient availability, leaf nutrient content, and photosynthetic capacity (Harrison et al. 2021). Leveraging a two-input microeconomics approach (Wright et al. 2003), the theory posits that plants acclimate to a given environment by optimizing leaf photosynthesis rates at the lowest summed cost of using nutrients and water (Prentice et al. 2014; Wang et al. 2017; Smith et al. 2019; Paillassa et al. 2020). Across resource availability gradients, the theory predicts that optimal photosynthetic rates can be achieved by trading less efficient use of a resource that is less costly to acquire (or more abundant) for more efficient use of a resource more costly to acquire (or less abundant). For example, an increase in soil nutrient availability should reduce the cost of acquiring and using nutrients (Bae et al. 2015; Eastman et al. 2021; Perkowski et al. 2021), which could increase leaf nutrient investments in photosynthetic proteins to allow similar photosynthetic rates to be achieved with higher nutrient use (lower nutrient use efficiency) but lower water use (greater water use efficiency). The

theory suggests similar tradeoffs in response to increasing soil pH (Paillassa et al. 2020), specifically, that increasing soil pH should reduce the cost of acquiring soil nutrients due to an increase in plant-available nutrient concentration (Paillassa et al. 2020; Dong et al. 2022). The theory is also capable of reconciling dynamic leaf nutrient-photosynthesis relationships at global scales (Luo et al. 2021).

Patterns expected from photosynthetic least-cost theory have recently received empirical support both in global environmental gradient (Smith et al. 2019; Paillassa et al. 2020; Luo et al. 2021; Querejeta et al. 2022; Westerband et al. 2023) and local manipulative invasion (Bialic-Murphy et al. 2021) studies. However, nutrient addition experiments that directly examine nutrient-water use tradeoffs expected from the theory are rare (Guerrieri et al. 2011), and only global gradient studies testing the theory have considered soil pH in their analyses. As a result, there is a need to use nutrient addition and soil pH manipulation experiments to test mechanisms driving responses predicted by the theory. Such experiments would also be useful to detect whether patterns expected from theory translate to finer spatial scales.

In this study, we measured leaf responses to soil N availability in five deciduous tree species growing in the upper canopy of mature closed canopy temperate forests in the northeastern United States. Soil N availability and pH were manipulated through a N-by-pH field manipulation experiment with treatments applied since 2011, eight years prior to measurement. Two different soil N treatments were applied to increase N availability with opposing effects on soil pH. An additional N-free acidifying treatment was expected to decrease soil pH. We hypothesized that increased soil N availability would enable plants to increase nutrient uptake

and create more photosynthetic enzymes per leaf, allowing similar photosynthetic rates achieved with lower leaf C_i:C_a and increased leaf N content allocated to photosynthetic leaf tissue. We expected that this response would be driven by a reduction in the cost of acquiring N, which would cause trees to sacrifice efficient N use to enable more efficient use of other limiting resources (i.e., water). We hypothesized similar leaf responses to increasing soil pH.

3.2 Methods

3.2.1 *Study site description*

We conducted this study in summer 2019 at three stands located within a 20-km radius of Ithaca, NY, USA (42.444 °N, 76.502 °W). All stands contain mature, closed-canopy forests dominated by deciduous tree species. Stands contained abundant sugar maple (*Acer saccharum* Marshall), American beech (*Fagus grandifolia* Ehrh.), and white ash (*Fraxinus americana* L.), accounting for 43%, 15%, and 17% of the total aboveground biomass across the three stands, respectively, with less frequent red maple (*Acer rubrum* L.; 9% of total aboveground biomass) and red oak occurrences (*Quercus rubra* L.; 10% of total aboveground biomass). Soils at each site were broadly classified as a channery silt loam Inceptisols using the USDA NRCS Web Soil Survey data product (Soil Survey Staff 2022). Between 2006 and 2020, study sites averaged 972 mm of precipitation per year and had an average temperature of 7.9 °C per a weather station located near the Cornell University campus (42.449 °N, 76.449 °W) part of the NOAA NCEI Global Historical Climatology Network (Menne et al. 2012).

3.2.2 *Experimental design*

Four 40 m x 40 m plots were set up at each site in 2009, each with an additional 10 m buffer along plot perimeters (60 m x 60 m total). The plots were set up as a nitrogen-by-pH field manipulation experiment, with one each of four treatments at each site. Two nitrogen treatments were applied, both at 50 kg N ha^{-1} yr^{-1}, as either sodium nitrate ($NaNO_3$) to raise soil pH, or ammonium sulfate ($(NH_4)_2SO_4$) to acidify; an elemental sulfur treatment was selected to acidify without N, applied at the same rate of S addition (57 kg S ha^{-1} yr^{-1}); and control plots received no additions. All amendments were added in pelletized form using hand-held fertilizer spreaders to both the main plots and buffers. Amendments were divided into three equal doses distributed across the growing season from 2011-2017 and added as a single dose from 2018 onward. During 2019, plots were fertilized during the week of May 20.

3.2.3 *Leaf gas exchange and trait measurements*

We sampled one leaf each from 6 to 10 individuals per plot between June 25 and July 12, 2019 for gas exchange measurements (Table S1). Leaves were collected from deciduous broadleaf trees represented across all sites and plots and were replicated in efforts to mimic the species abundance of each plot at each site. We also attempted to collect leaves from the upper canopy to reduce differential shading effects on leaf physiology. Leaves were accessed by pulling down small branches using an arborist's slingshot and weighted beanbag attached to a throwline. Branches were immediately recut under deionized water and remained submerged to reduce stomatal closure and avoid xylem embolism (as in Smith &

Dukes, 2018) until gas exchange data were collected.

Randomly selected leaves with little to no visible external damage were attached to a Li-COR LI-6800 (Li-COR Bioscience, Lincoln, Nebraska, USA) portable photosynthesis machine to measure net photosynthesis (A_{net}; μmol m^{-2} s^{-1}), stomatal conductance (g_{sw}; mol m^{-2} s^{-1}), and intercellular CO_2 concentration (C_{i}; μmol mol^{-1}) at different reference CO_2 concentrations (C_{a}; μmol mol^{-1}) concentrations (i.e., an $A_{\text{net}}/C_{\text{i}}$ curve) under saturating light conditions (2,000 μmol m^{-2} s^{-1}). Reference CO_2 concentrations followed the sequence: 400, 300, 200, 100, 50, 400, 400, 600, 800, 1000, 1200, 1500, and 2000 μmol mol^{-1} CO_2. Leaf temperatures were not controlled in the cuvette and ranged from 21.8 °C to 31.7 °C (mean±SD: 27.2 ± 2.2 °C). A linear and second order log-polynomial nonlinear regression suggested no effect of temperature on stomatal conductance measured at 400 μmol mol^{-1} CO_2 or net photosynthesis measured at μmol mol^{-1} CO_2 (Table S2-3; Fig. S1). All $A_{\text{net}}/C_{\text{i}}$ curves were generated within one hour of branch severance.

Leaf morphological and chemical traits were collected on the same leaf used to generate each Anet/Ci curve. Images of each leaf were taken using a flat-bed scanner to determine fresh leaf area using the 'LeafArea' R package (Katabuchi 2015), which automates leaf area calculations using ImageJ software (Schneider et al. 2012). Each leaf was dried at 65°C for at least 48 hours, weighed, and ground using a Retsch MM200 ball mill grinder (Verder Scientific, Inc., Newtown, PA, USA) until homogenized. Leaf mass per area (M_{area}, g m^{-2}) was calculated as the ratio of dry leaf biomass to fresh leaf area. Using a subsample of ground and homogenized leaf biomass, leaf N content (N_{mass}; gN g^{-1}) and leaf δ^{13}C (‰, rela-

tive to VPDB) were measured at the Cornell Stable Isotope Lab with an elemental analyzer (NC 2500, CE Instruments, Wigan, UK) interfaced to an isotope ratio mass spectrometer (Delta V Isotope Ratio Mass Spectrometer, ThermoFisher Scientific, Waltham, MA, USA). Leaf N content per unit leaf area (N_{area}; gN m^{-2}) was calculated by multiplying N_{mass} by M_{area}.

We used leaf δ^{13}C values to estimate χ (unitless), which is an isotope-derived estimate of the leaf C_{i}:C_{a} ratio. While intercellular and atmospheric CO_2 concentrations were directly measured during each $A_{\text{net}}/C_{\text{i}}$ curve, deriving χ from δ^{13}C provides a more integrative estimate of the C_{i}:C_{a} over an individual leaf's lifespan. We derived χ following the approach of Farquhar et al. (1989) decribed in Cernusak et al. (2013):

$$\chi = \frac{\Delta^{13}C - a}{b - a} \tag{3.1}$$

where Δ^{13}C represents the relative difference between leaf δ^{13}C (‰) and air δ^{13}C (‰), and is calculated from the following equation:

$$\Delta^{13}C = \frac{\delta^{13}C_{air} - \delta^{13}C_{leaf}}{1 + \delta^{13}C_{leaf}} \tag{3.2}$$

where $\delta^{13}\text{C}_{\text{air}}$ is assumed to be -8‰ (Keeling et al. 1979; Farquhar et al. 1989), a represents the fractionation between ^{12}C and ^{13}C due to diffusion in air, assumed to be 4.4‰, and b represents the fractionation caused by Rubisco carboxylation, assumed to be 27‰ (Farquhar et al. 1989).

3.2.4 *A_{net}/C_i curve-fitting and parameter estimation*

We fit $A_{\text{net}}/C_{\text{i}}$ curves of each individual using the 'fitaci' function in the 'plantecophys' R package (Duursma 2015). This function estimates the maximum rate of Rubisco carboxylation V_{cmax}; μmol m^{-2} s^{-1}) and maximum rate of electron transport for RuBP regeneration (J_{max}; μmol m^{-2} s^{-1}) based on the Farquhar, von Caemmerer, and Berry biochemical model of C_3 photosynthesis (Farquhar et al. 1980). For each curve fit, we included triose phosphate utilization (TPU) limitation to avoid underestimating J_{max} (Gregory et al. 2021). Curves were visually examined to confirm the likely presence of TPU limitation.

We determined Michaelis-Menten coefficients for Rubisco affinity to CO_2 (K_{c}; μmol mol^{-1}) and O_2 (K_{o}; μmol mol^{-1}), and the CO_2 compensation point (Γ^*; μmol mol^{-1}) using leaf temperature and equations described in Medlyn et al. (2002) and derived in Bernacchi et al. (2001). Specifically, K_{c} and K_{o} were calculated as:

$$K_{\text{c}} = 404.9 * exp^{\frac{79430(T_{\text{k}}-298)}{298RT_{\text{k}}}} \tag{3.3}$$

and

$$K_{\text{o}} = 278.4 * exp^{\frac{36380(T_{\text{k}}-298)}{298RT_{\text{k}}}} \tag{3.4}$$

while Γ^* was calculated as:

$$\Gamma^* = 42.75 * exp^{\frac{37830(T_{\text{k}}-298)}{298RT_{\text{k}}}} \tag{3.5}$$

600 In all three equations, T_{k} is the leaf temperature (in Kelvin) during each $A_{\mathrm{net}}/C_{\mathrm{i}}$
601 curve and R is the universal gas constant (8.314 J mol^{-1} K^{-1}).

602 We standardized V_{cmax} and J_{max} estimates to 25 °C using a modified Ar-
603 rhenius equation (Kattge and Knorr 2007):

$$k_{25} = \frac{k_{\mathrm{obs}}}{e^{\frac{Ha(T_{obs}-T_{ref})}{T_{ref}RT_{obs}}} * \frac{1+e^{\frac{T_{ref}\Delta S-H_d}{T_{ref}}}}{1+e^{\frac{T_{obs}\Delta S-H_d}{T_{obs}}}}} \tag{3.6}$$

604 k_{25} represents the standardized V_{cmax} or J_{max} rate at 25°C, kobs represents
605 the V_{cmax} or J_{max} estimate at the average leaf temperature measured inside the
606 cuvette during the $A_{\mathrm{net}}/C_{\mathrm{i}}$ curve. H_{a} is the activation energy of V_{cmax} (71,513
607 J mol^{-1}) Kattge and Knorr (2007) or J_{max} (49,884 J mol^{-1}) (Kattge and Knorr
608 2007). H_{d} represents the deactivation energy of both V_{cmax} and J_{max} (200,000 J
609 mol-1) (Medlyn et al. 2002), and R represents the universal gas constant (8.314
610 J mol^{-1} K^{-1}). T_{ref} represents the standardized temperature of 298.15 K (25°C)
611 and T_{obs} represents the mean leaf temperature (in K) during each $A_{\mathrm{net}}/C_{\mathrm{i}}$ curve.
612 ΔS is an entropy term that (Kattge and Knorr 2007) derived as a linear relation-
613 ship with average growing season temperature (T_{g}; °C), where:

$$\Delta S_{vcmax} = -1.07\ T_g + 668.39 \tag{3.7}$$

614 and

$$\Delta S_{jmax} = -0.75\ T_g + 659.70 \tag{3.8}$$

We estimated T_{g} in Equations 3.7 and 3.8 based on mean daily (24-hour) air temperature of the 30 days leading up to the day of each sample collection using the same weather station reported in the site description. We then used V_{cmax25} and J_{max25} estimates to calculate the ratio of J_{max25} to V_{cmax25} (J_{max25}:V_{cmax25}; unitless).

3.2.5 *Proportion of leaf nitrogen allocated to photosynthesis and structure*

We used equations from Niinemets and Tenhunen (1997) to estimate the proportion of leaf N content allocated to Rubisco and bioenergetics. The proportion of leaf N allocated to Rubisco (ρ_{rub}; gN gN^{-1}) was calculated as a function of V_{cmax25} and N_{area}:

$$\rho_{rubisco} = \frac{V_{cmax25} N_r}{V_{cr} N_{area}} \tag{3.9}$$

where N_{r} is the amount of nitrogen in Rubisco, set to 0.16 gN (gN in Rubisco)$^{-1}$ and V_{cr} is the maximum rate of RuBP carboxylation per unit Rubisco protein, set to 20.5 μmol CO_2 (g Rubisco)$^{-1}$. The proportion of leaf nitrogen allocated to bioenergetics (ρ_{bioe}; gN gN^{-1}) was similarly calculated as a function of J_{max25} and N_{area}:

$$\rho_{bioe} = \frac{J_{max25} N_b}{J_{mc} N_{area}} \tag{3.10}$$

where N_{b} is the amount of nitrogen in cytochrome f, set to 0.12407 gN (μmol cytochrome f)$^{-1}$ assuming a constant 1: 1: 1.2 cytochrome f: ferredoxin NADP reductase: coupling factor molar ratio (Evans and Seemann 1989; Niinemets and

633 Tenhunen 1997), and J_{mc} is the capacity of electron transport per cytochrome f,
634 set to 156 μmol electron (μmol cytochrome f)$^{-1}$s^{-1}.

635 We estimated the proportion of leaf N content allocated to photosynthetic
636 tissue (ρ_{photo}; gN gN^{-1}) as the sum of ρ_{rub} and ρ_{bioe}. This calculation is an un-
637 derestimate of the proportion of leaf N allocated to photosynthetic tissue because
638 it does not include N allocated to light harvesting proteins. This leaf N pool was
639 not included because we did not perform chlorophyll extractions on focal leaves.
640 However, the proportion of leaf N content allocated to light harvesting proteins
641 tends to be small relative to ρ_{rub} and ρ_{bioe}, and may scale with changes in ρ_{rub}
642 and ρ_{bioe} (Niinemets and Tenhunen 1997).

643 Finally, we estimated the proportion of leaf N content allocated to struc-
644 tural tissue (ρ_{str}; gN gN^{-1}) using an empirical equation from Onoda et al. (2017):

$$N_{cw} = 0.000355 * {M_{area}}^{1.39} \tag{3.11}$$

645 where N_{cw} is the leaf N content allocated to cell walls (gN m^{-2}). ρ_{str} was estimated
646 by dividing N_{cw} by N_{area}.

647 3.2.6 *Tradeoffs between nitrogen and water use*

648 Photosynthetic nitrogen use efficiency (PNUE; μmol CO$_2$ mol^{-1} N s^{-1})
649 was calculated by dividing A_{net} by N_{area}, first converting N_{area} to mol N m^{-2}
650 using the molar mass of N (14 g mol^{-1}). We used χ as an indicator of water
651 use efficiency, which exploratory analyses suggest had similar responses to soil N
652 availability and pH as intrinsic water use efficiency measured from gas exchange

653 ($A_{\text{net}}/g_{\text{s}}$). Tradeoffs between nitrogen and water use were determined by cal-
654 culating the ratio of N_{area} to χ (N_{area}:χ; g N m^{-2}) and V_{cmax25} to χ (V_{cmax25}:χ;
655 μmol m^{-2} s^{-1}). This approach is similar to tradeoff calculations in which nitrogen-
656 water use tradeoffs are measured as the ratio of N_{area} or V_{cmax25} to g_{s} (Paillassa
657 et al. 2020; Bialic-Murphy et al. 2021). In this study, we quantify these re-
658 lationships using χ in lieu of g_{s} because g_{s} rapidly changes with environmental
659 conditions and therefore may have been altered by recent tree branch severance
660 and/or placement in the cuvette.

661 3.2.7 *Soil nitrogen availability and pH*

662 To characterize soil N availability at the time of our leaf gas exchange
663 measurements, we used mixed bed resin bags to quantify mobile ammonium-N
664 and nitrate-N concentrations in each plot. Lycra mesh bags were filled with 5 g
665 of Dowex® Marathon MR-3 hydrogen and hydroxide form resin (MilliporeSigma,
666 Burlington, MA USA) and sealed with a zip tie. Each bag was activated by
667 soaking in 0.5 M HCl for 20 minutes, then in 2 M NaCl until pH of the saline
668 solution stabilized, as described in Allison et al. (2008). Five resin bags were
669 inserted about 10 cm below the soil surface at each plot on June 25, 2019: one
670 near each of the four plot corners and one near the plot center. All resin bags
671 were collected 24 days later on July 19, 2019 and were frozen until extracted.

672 Prior to anion and cation extraction, each resin bag was rinsed with ul-
673 trapure water (MilliQ IQ 7000; Millipore Sigma, Burlington, MA) to remove any
674 surface soil residues. Anions and cations were extracted from surface-cleaned resin
675 bags by individually soaking and shaking each bag in 100 mL of a 0.1 M HCl/2.0

M NaCl matrix for one hour. Using a microplate reader (Biotek Synergy H1; Biotek Instruments, Winooski, VT USA), nitrate-N concentrations were quantified spectrophotometrically at 540 nm with the end product of a single reagent vanadium (III) chloride reaction (Doane and Horwáth 2003), and ammonium-N concentrations quantified at 650 nm with the end product of a modified phenol-hypochlorite reaction (Weatherburn 1967; Rhine et al. 1998). Both the single reagent vanadium (III) chloride and modified phenol-hypochlorite methodologies have been well established for determining nitrate-N and ammonium-N concentrations in resin bag extracts (Arnone 1997; Allison et al. 2008). We used a series of negative and positive controls throughout each well plate to verify the accuracy and precision of our measurements, assaying each resin bag extract and control in triplicate. Soil N availability was estimated as the sum of the nitrate-N and ammonium-N concentration in each resin bag, normalized per g of resin and duration in the field (μg N g^{-1} resin d^{-1}), then subsequently averaged across all resin bags in a plot for a plot-level mean.

Soil pH was measured on 0-10 cm mineral soil samples collected prior to fertilization in 2019. Near each of the four plot corners, three 5.5 cm diameter soil cores were collected after first removing the forest floor where present. Each set of three cores was placed in a plastic bag, and later composited by hand mixing and sieved to 4mm. Soil pH was determined for a 1:2 soil:water slurry (10 g field-moist soil to 20 mL DI water) of each sample using an Accumet AB15 pH meter with flushable junction probe (Fisher Scientific; Hampton, NH, USA), and was estimated at the plot level as the mean soil pH within each plot.

3.2.8 *Statistical analyses*

We built two separate series of linear mixed-effects models to explore effects of soil N availability, soil pH, species, and leaf N content on leaf physiological traits. In the first series of linear mixed-effects models, we explored the effect of soil N availability, soil pH, and species on leaf N content, leaf photosynthesis, stomatal conductance, and nitrogen-water use tradeoffs. Models included plot-level soil N availability and plot-level soil pH as continuous fixed effects, species as a categorical fixed effect, and site as a categorical random intercept term. Interaction terms between fixed effects were not included due to the small number of experimental plots. We built a series of separate models with this independent variable structure to quantify individual effects of soil N availability, soil pH, and species on N_{area}, M_{area}, N_{mass}, A_{net}, V_{cmax25}, J_{max25}, J_{max25}:V_{cmax25}, ρ_{rubisco}, $\rho_{\text{bioenergetics}}$, ρ_{photo}, $\rho_{\text{structure}}$, χ, PNUE, N_{area}:χ, and V_{cmax25}:χ.

A second series of linear mixed-effects models were built to investigate relationships between leaf N content and photosynthetic parameters. Statistical models included Narea as a single continuous fixed effect with species and site designated as individual random intercept terms. We used this independent variable structure to quantify individual effects of leaf N content on A_{net}, V_{cmax25}, J_{max25}, J_{max25}:V_{cmax25}, and χ.

For all linear mixed-effects models, we used Shapiro-Wilk tests of normality to determine whether linear mixed-effects models satisfied residual normality assumptions. If residual normality assumptions were not met, then models were fit using dependent variables that were natural log transformed. If residual normality assumptions were still not met (Shapiro-Wilk: $p < 0.05$), then models were

fit using dependent variables that were square root transformed. All residual normality assumptions for both sets of models that did not originally satisfy residual normality assumptions were met with either a natural log or square root data transformation (Shapiro-Wilk: $p > 0.05$ in all cases).

In the first series of models, models for N_{area}, M_{area}, N_{mass}, V_{cmax25}, J_{max25}, χ, N_{area}:χ, and V_{cmax25}:χ, ρ_{rubisco}, $\rho_{\text{bioenergetics}}$, ρ_{photo}, $\rho_{\text{structure}}$ satisfied residual normality assumptions without data transformations (Shapiro-Wilk: $p > 0.05$ in all cases). The model for J_{max25}:V_{cmax25} satisfied residual normality assumptions with a natural log data transformation, while models for A_{net} and PNUE each satisfied residual normality assumptions with square root data transformations. In the second series of models, models for V_{cmax25}, J_{max25}, χ, and V_{cmax25}:χ satisfied residual normality assumptions without data transformations (Shapiro-Wilk: $p > 0.05$ in all cases). The model for J_{max25}:V_{cmax25} required a natural log data transformation and the model for Anet required a square root data transformation (Shapiro-Wilk: $p > 0.05$ in both cases).

In all models, we used the 'lmer' function in the 'lme4' R package (Bates et al. 2015) to fit each model and the 'Anova' function in the 'car' R package (Fox and Weisberg 2019) to calculate Type II Wald's χ^2 and determine the significance level ($\alpha = 0.05$) of each fixed effect coefficient. Finally, we used the 'emmeans' R package (Lenth, 2019) to conduct post-hoc comparisons using Tukey's tests, where degrees of freedom were approximated using the Kenward-Roger approach (Kenward and Roger 1997). All analyses and plots were conducted in R version 4.1.1 (R Core Team 2021)). All figure regression lines and associated 95% confidence interval error bars were plotted using predictions generated across the soil

nitrogen availability gradient using the 'emmeans' R package (Lenth 2019).

3.3 Results

3.3.1 *Leaf N content*

Increasing soil N availability generally increased N_{area} (Table 3.1; Fig. 3.1a). This pattern was driven by an increase in N_{mass} (Table 3.1; Fig. 3.1c) and a marginal increase in Marea (Table 1; Fig. 1e) with increasing soil N availability. There was no effect of soil pH on N_{area}, N_{mass}, or M_{area} (Table 1); however, we did observe strong differences in N_{area} (Fig. 1b), N_{mass} (Fig. 1d), and M_{area} (Fig. 1e) between species (Table 1).

756 [placeholder for Table 1]

757 [placeholder for Fig 1]

3.3.2 *Net photosynthesis and leaf biochemistry*

Increasing soil N availability generally had no effect on A_{net}, V_{cmax25}, J_{max25}, or J_{max25}:V_{cmax25} (Figs. 2a, 2d, 2g). We also observed strong species effects on all measured leaf photosynthetic traits (Table 2; Figs. 2b, 2e, 2h). Increasing soil pH had a marginal negative effect on A_{net}, but had no effect on V_{cmax25}, J_{max25}, or J_{max25}:V_{cmax25}(Table 2). There was a weak positive effect of increasing N_{area} on A_{net} (Fig. 2c), but quite strong positive effects of increasing N_{area} on V_{cmax25} and J_{max25} (Table 2; Fig. 2f and 2i).

766 [placeholder for Table 2]

767 [placeholder for Fig 2]

3.3.3 *Leaf N allocation*

Neither soil N availability nor soil pH affected the proportion of leaf N allocated to Rubisco or bioenergetics (Table 3; Fig. 3a, Fig. 3c), nor was there any subsequent effect on the proportion of leaf N allocated to photosynthesis (Table 3; Fig. 3f). We also found no effect of soil N availability or soil pH on the proportion of leaf N allocated to structure (Table 3; Fig 3g). Species varied in the proportion of leaf N allocated to Rubisco, photosynthesis, and structure (Fig 3b, Fig. 3d, Fig 3h), with no detectable species effect on the proportion of leaf N allocated to bioenergetics (Table 3).

777 [placeholder for Table 3]

778 [placeholder for Fig 3]

3.3.4 *Tradeoffs between nitrogen and water use*

Although soil N availability did not affect χ (Table 4; Fig. 4a), increasing soil N availability decreased PNUE (Table 4; Fig. 4d) and increased the ratio of N_{area}:χ (Table 4; Fig. 4f). Specifically, this response yielded a 26% reduction in PNUE and 37% stimulation in N_{area}:χ across the soil nitrogen availability gradient. There was no apparent effect of soil N availability on V_{cmax25}:χ (Table 4; Fig. 4h). Increasing soil pH had a weak marginal negative effect on PNUE, but did not influence χ, N_{area}:χ, or V_{cmax25}:χ (Table 4). We also observed differences in χ (Fig. 4b), PNUE (Fig. 4e), N_{area}:χ (Fig. 4g), and V_{cmax25}:χ (Fig. 4i) between species (Table 4). Finally, increasing N_{area} had a strong negative effect on χ (Table 4; Fig. 4c) and a strong positive effect on V_{cmax25}:χ (Table 4; Fig. 4j).

790 [placeholder for Table 4]

791 [placeholder for Fig 4]

3.4 Discussion

Photosynthetic least-cost theory provides an explanation for understanding relationships between soil nutrient availability, leaf nutrient allocation, and photosynthetic capacity. The theory suggests that plants acclimate to a given environment by optimizing leaf photosynthesis rates at the lowest summed cost of using nutrients and water Prentice et al. (2014), Wang et al. (2017), Smith et al. (2019), Paillassa et al. (2020). The theory predicts that an increase in soil nutrient availability should allow similar photosynthesis rates to be achieved with increased leaf nutrient content and photosynthetic capacity (i.e., V_{cmax25} and J_{max25}) at lower leaf C_{i}:C_{a} (χ), resulting in an increase in water use efficiency, decrease in nutrient use efficiency, and increase in both leaf nutrient content and photosynthetic capacity per unit χ. The theory predicts similar leaf responses to increasing soil pH under acidic conditions, presumably due to generally faster nutrient cycle dynamics and consequent reductions in the cost of acquiring nutrients relative to water with increasing soil pH (Wang et al. 2017; Paillassa et al. 2020; Dong et al. 2020).

Supporting the theory, we showed that increasing soil N availability was associated with increased leaf N content (Fig 3.1a, 3.1c), a pattern that reduced photosynthetic N use efficiency (Fig 3.4d) and increased leaf N content per unit χ (Fig 3.4f). Increasing soil N coincided with slight, but non-significant decreases in χ and increases in V_{cmax25} and J_{max25} ($p < 0.2$). The positive trend between soil N availability and photosynthetic capacity was supported by the concurrent strong increase in leaf N content with increasing soil N availability, which resulted in no change in the proportion of leaf N content allocated to photosynthesis across

the soil N availability gradient. Additionally, leaf N content exhibited a strong negative correlation with χ, indicative of strong nitrogen-water use tradeoffs at the leaf level. Responses tended to vary more due to soil N availability than soil pH. Overall, these findings are consistent with the nutrient-water use tradeoffs predicted from theory.

3.4.1 *Soil nitrogen availability modifies tradeoffs between nitrogen and water use*

In support of expected least-cost outcomes and past environmental gradient studies (Dong et al. 2017; Paillassa et al. 2020), we found that increasing soil N availability was associated with increased leaf N content. Soil N availability had smaller impacts on measures of net photosynthesis and χ, which led to reductions in PNUE and increases in leaf N content per unit χ, as expected from theory. Photosynthetic least-cost theory suggests that reductions in PNUE should be driven by an increase in the proportion of leaf N allocated to photosynthetic tissue, a pattern that should allow plants to achieve optimal photosynthetic rates with greater photosynthetic capacity to make better use of available light. Contrasting theory predictions, we found no effect of soil N availability on photosynthetic capacity. However, photosynthetic capacity did tend to increase with increasing soil N availability ($p < 0.20$; Table 2) resulting in no effect of soil N availability on the relative fraction of leaf N allocated to photosynthesis, Rubisco, or bioenergetics (Fig. 3). These lines of evidence support the idea that trees use additional N to support increased leaf N allocation toward photosynthetic tissue and enhance photosynthetic capacity (Wright et al. 2003).

Soil N availability had a stronger effect on leaf N than photosynthetic ca-

839 pacity. This pattern suggests that additional plant N uptake due to increased
840 soil N availability was also being used to support non-photosynthetic N pools,
841 possibly to structural tissue or stress-induced amino acid and polyamine synthe-
842 sis (Minocha et al. 2000; Onoda et al. 2004; Bubier et al. 2011). While we
843 found no change in the proportion of leaf N allocated to leaf structural tissue, the
844 overall stimulation in leaf N content with increasing soil N availability suggests an
845 increase in the net amount of N invested in leaf structural tissue along the N avail-
846 ability gradient. Importantly, leaf N allocated to structure was calculated using
847 an empirical relationship between M_{area} and the amount of leaf N allocated to cell
848 walls (Onoda et al. 2017). As the generality of relationships between Marea and
849 the amount of leaf N allocated to cell walls has been called into question (Harrison
850 et al. 2009), future work should consider explicitly measuring N allocation to cell
851 wall tissue and stress-induced amino acid synthesis to confirm these patterns.

852 In opposition to patterns expected from least cost theory, increasing soil
853 N availability had no apparent effect on χ (Fig. 4a). Interestingly, despite the
854 null effect of soil N availability on χ, we observed a strong negative effect of
855 increasing Narea on χ (Fig. 4c), consistent with the nitrogen-water use tradeoffs
856 expected from theory. The null response of χ to increasing soil N availability may
857 have been due to a lack of water limitation in the system, given that the area
858 received approximately 20% more precipitation (1167 mm) during the 12-month
859 period leading up to our measurement period than normally expected (972 mm).
860 However, droughts can and do occur in temperate forests of the northeastern
861 United States (Sweet et al. 2017), so the observed increase in leaf N content
862 with increasing soil N availability could be a strategy that allows trees to hedge

bets against drier than normal growing seasons (Onoda et al. 2004; Onoda et al. 2017; Hallik et al. 2009). As was suggested in Paillassa et al. (2020), and more recently by Querejeta et al. (2022), negative effects of soil N availability on χ may increase with increasing aridity. This strategy would be especially advantageous if it allows individuals growing in arid regions to maintain carbon assimilation rates with reduced water loss. Future work should attempt to quantify interactive roles of climate and soil nitrogen availability on nitrogen-water use tradeoffs, which could be done by leveraging coordinated and multi-factor nutrient (Borer et al. 2014) and water (Knapp et al. 2017) manipulation experiments across broad climatic gradients.

3.4.2 *Soil pH did not modify tradeoffs between nitrogen and water usage*

While the primary purpose of this study was to examine the role of soil N availability on nitrogen-water use tradeoffs, our experimental design manipulated both soil N and pH, providing an opportunity to isolate the roles of these variables. Previous correlational studies along environmental gradients identified soil pH as a particularly important factor that can modify tradeoffs between nutrient and water use (Smith et al. 2019; Paillassa et al. 2020; Westerband et al. 2023) and the proportion of leaf nitrogen allocated to photosynthesis (Luo et al. 2021). Such studies implied that these patterns may be driven by reductions in the cost of acquiring nutrients relative to water with increasing pH, which may be exacerbated in acidic soils.

Consistent with theory (Wright et al. 2003; Prentice et al. 2014), our results indicate that increasing soil pH was negatively associated with PNUE.

However, there was no effect of soil pH on leaf N content, χ, or leaf N content per unit χ, most likely because the experimental N additions increased soil N supply while both increasing (sodium nitrate) and decreasing (ammonium sulfate) soil pH. These results suggest that soil pH did not play a major role in modifying expected photosynthetic least-cost theory patterns, contrasting findings from Paillassa et al. (2020) and other gradient studies that note positive effects of increasing soil pH on leaf N content, Rubisco carboxylation, and χ (Viet et al. 2013; Cornwell et al. 2018; Luo et al. 2021). Instead, null responses to soil pH show that leaf photosynthetic parameters depend more on soil N availability than pH per se, and that inferences from gradient studies might be confounding covariation between N availability and soil acidity.

3.4.3 *Species identity explains a large amount of variation in leaf and whole plant traits*

Species generally explained a larger amount of variation in measured leaf traits than soil N availability or soil pH. Interspecies variation is an important factor to consider when deducing mechanisms that drive photosynthetic least-cost theory, particularly for species that form distinct mycorrhizal associations or have different photosynthetic pathways, growth forms, or leaf habit (Espelta et al. 2005; Adams et al. 2016; Bialic-Murphy et al. 2021; Scott and Smith 2022). The need to consider species may also be important when comparing nutrient-water use tradeoffs in early and late successional species, or in species with different resource economic strategies (Abrams and Mostoller 1995; Ellsworth and Reich 1996; Wright et al. 2004; Reich 2014; Onoda et al. 2017; Ziegler et al. 2020).

A strength of the study design and sampling effort is that it controls for many species differences that should modify nitrogen-water use tradeoffs expected from theory. All tree species measured in this study shared the leaf habit of deciduous broadleaves, were growing in forests of similar successional stage, but differed in mycorrhizal association and consequent resource economic strategies. As stands tended to be dominated by trees that associate with arbuscular mycorrhizae (*Fraxinus* and both *Acer* species made up 70% of total aboveground biomass across stands), ecosystem biogeochemical cycle dynamics may be more closely aligned to the inorganic nutrient economy proposed in Phillips et al. (2013), which may promote stronger nitrogen-water use tradeoffs in tree species that associate with arbuscular mycorrhizae. This result was not observed here, as photosynthetic properties varied as much within as across the two mycorrhizal associations represented. Given the high variability in measured photosynthetic traits within and across species, effects of mycorrhizal association likely require more intensive sampling efforts to detect than were possible here.

3.4.4 *Implications for photosynthetic least-cost theory model development*

In the field, soil nutrient availability is heterogeneous across time and space (Table S4). Unaccounted within-plot heterogeneity may have contributed to the low amount of variation explained by soil N availability in our statistical models, as resin bags are a coarse surrogate for soil N availability. Despite this, we still observed evidence for nutrient-water use tradeoffs, suggesting that observed responses reported here may be an underestimate toward the net effect of soil N availability on these tradeoffs. While we urge caution in the interpretation of

these results, they do provide a promising baseline for future studies investigating patterns expected from photosynthetic least-cost theory at finer spatiotemporal resolutions.

The general stronger relationship between leaf N content and photosynthetic parameters versus between leaf N content and soil N availability suggests that leaf N content is more directly tied to photosynthesis than soil N availability. While this could be due to the high spatiotemporal heterogeneity of soil N availability, principles from photosynthetic least-cost theory suggest that leaf N content is the downstream product of leaf nutrient demand to build and maintain photosynthetic machinery, which is set by aboveground environmental conditions such as light availability, CO2, temperature, or vapor pressure deficit (Smith et al. 2019; Paillassa et al. 2020; Peng et al. 2021; Westerband et al. 2023). The stronger relationship between leaf N and photosynthetic parameters paired with the strong negative relationship between leaf N and χ could indicate a relatively stronger effect of climate on leaf N-photosynthesis relationships than soil resource availability. However, the short distance between plots and across sites limited our ability to test this mechanism.

Variation in soil pH affected least cost responses less than variations in soil N availability, in part because experimental treatments directly increased soil N and affected soil pH in opposite directions. While soil pH has been shown to drive nitrogen-water tradeoffs in global gradient analyses (Viet et al. 2013; Paillassa et al. 2020), these responses may be due to covariations between soil pH and nutrient cycling rather than a role of pH per se. The direct manipulations of soil pH and soil N availability in this study allowed us to partly disentangle

these factors and show that variation in N availability matters more for least-cost tradeoffs than pH alone.

3.4.5 *Conclusions*

Increasing soil N availability generally increased leaf N content (both area- and mass-based), but did not significantly influence χ. This shift in leaf N led to a reduction in PNUE, and an increase in leaf N per unit χ with increasing soil N availability. Despite null effects of soil N availability on χ, we observed a strong negative relationship between leaf N content and χ. These results provide empirical support for the nutrient-water use tradeoffs expected from photosynthetic least-cost theory in response to soil nutrient availability, but suggest that all tenets of the theory may not hold in every environment. These results experimentally test previous work suggesting that leaf water-nitrogen economies vary across gradients of soil nutrient availability and pH, and show that variations in nutrient availability matter more for determining variation in leaf photosynthetic traits than soil pH.

Chapter 4

The relative cost of resource use for photosynthesis drives variance in leaf nitrogen content across climate and soil resource availability gradients

4.1 Introduction

Terrestrial biosphere models, which comprise the land surface component of Earth system models, are sensitive to the formulation of photosynthetic processes (Knorr 2000; Ziehn et al. 2011; Booth et al. 2012). This is because photosynthesis is the largest carbon flux between the atmosphere and terrestrial biosphere, and is constrained by ecosystem carbon and nutrient cycles (Hungate et al. 2003; LeBauer and Treseder 2008; IPCC 2021; Fay et al. 2015). Many terrestrial biosphere models formulate photosynthesis by parameterizing photosynthetic capacity within plant functional groups through empirical linear relationships between area-based leaf nitrogen content (N_{area}) and the maximum carboxylation rate of Ribulose-1,5-bisphosphate carboxylase/oxygenase (Kattge et al. 2009; Rogers 2014; Rogers et al. 2017). Models are also beginning to include connected carbon-nitrogen cycles (Wieder et al. 2015; Shi et al. 2016; Davies-Barnard et al. 2020; Braghiere et al. 2022), which allows leaf photosynthesis to be predicted directly through changes in N_{area} and indirectly through changes in soil nitrogen availability (e.g., LPJ-GUESS, Smith et al., 2014; CLM5.0, Lawrence et al., 2019). Despite recent model developments, open questions remain regarding the generality of ecological relationships between soil nitrogen availability, leaf nitrogen content, and leaf photosynthesis across edaphic and climatic gradients.

Empirical support for positive relationships between soil nitrogen avail-

ability and N_{area} is abundant (Firn et al. 2019; Liang et al. 2020), and is a result often attributed to the high nitrogen cost of building and maintaining Rubisco (Evans 1989; Evans and Seemann 1989; Onoda et al. 2004; Onoda et al. 2017; Dong et al. 2020). Such patterns imply that positive relationships between soil nitrogen availability and N_{area} should cause an increase in leaf photosynthesis and photosynthetic capacity by increasing the maximum rate of Rubisco carboxylation through increased investments to Rubisco construction and maintenance. This integrated N_{area}-photosynthesis response to soil nitrogen availability has been observed both in manipulative experiments and across environmental gradients (Field and Mooney 1986; Evans 1989; Walker et al. 2014; Li et al. 2020), and is thought to be driven by ecosystem nitrogen limitation, which limits primary productivity globally (LeBauer and Treseder 2008; Fay et al. 2015). However, this response is not consistently observed, as recent studies note variable N_{area}-photosynthesis relationships across soil nitrogen availability gradients (Liang et al. 2020; Luo et al. 2021) and that aboveground growing conditions (e.g., light availability, temperature, vapor pressure deficit) or species identity traits (e.g., photosynthetic pathway, nitrogen acquisition strategy) may be more important for explaining variance in N_{area} and photosynthetic capacity across time and space (Adams et al. 2016; Dong et al. 2017; Dong et al. 2020; Dong et al. 2022; Smith et al. 2019; Peng et al. 2021; Westerband et al. 2023).

4.2 Methods

4.3 Results

4.4 Discussion

Chapter 5

Optimal resource investment to photosynthetic capacity maximizes nutrient allocation to whole plant growth under elevated CO2

5.1 Introduction

Terrestrial ecosystems are regulated by complex carbon and nitrogen cycles. As a result, terrestrial biosphere models, which are beginning to include coupled carbon and nitrogen cycles (Shi et al. 2016; Davies-Barnard et al. 2020; Braghiere et al. 2022), must accurately represent these cycles under different environmental scenarios to reliably simulate carbon and nitrogen atmosphere-biosphere fluxes (Hungate et al. 2003; Prentice et al. 2015). While the inclusion of coupled carbon and nitrogen cycles tends to reduce model uncertainty (Arora et al. 2020), large uncertainty in role of soil nitrogen availability and nitrogen acquisition strategy on leaf and whole plant acclimation responses to CO_2 remains (Smith and Dukes 2013; Terrer et al. 2018; Smith and Keenan 2020). This source of uncertainty likely contributes to the widespread divergence in future carbon and nitrogen flux simulations across terrestrial biosphere models (Friedlingstein et al. 2014; Zaehle et al. 2014; Meyerholt et al. 2020).

Plants grown under elevated CO_2 generally have less leaf nitrogen content than those grown under ambient CO_2, a response that often corresponds with reductions in photosynthetic capacity and stomatal conductance at the leaf-level and biomass stimulation over time at the whole plant level (Curtis 1996; Drake et al. 1997; Ainsworth et al. 2002; Makino 2003; Morgan et al. 2004; Ainsworth and Long 2005; Ainsworth and Rogers 2007; Smith and Dukes 2013; Poorter et al. 2022). As net primary productivity is generally limited by nitrogen availability

(Vitousek and Howarth 1991; LeBauer and Treseder 2008; Fay et al. 2015), and soil nitrogen availability is often positively correlated with leaf nitrogen content and photosynthetic capacity (Field and Mooney 1986; Evans and Seemann 1989; Evans 1989; Walker et al. 2014; Firn et al. 2019; Liang et al. 2020), some have hypothesized that leaf and whole plant acclimation responses to CO_2 are constrained by soil nitrogen availability. The progressive nitrogen limitation hypothesis predicts that elevated CO_2 will increase plant nitrogen demand, which will increase plant nitrogen uptake and progressively deplete soil nitrogen if soil nitrogen supply does not exceed plant nitrogen demand (Luo et al. 2004). The hypothesis predicts that this response should result in strong acute stimulations in whole plant growth and primary productivity that diminish over time as nitrogen becomes more limiting. Assuming a positive relationship between soil nitrogen availability, leaf nitrogen content, and photosynthetic capacity, this hypothesis also implies that progressive reductions in soil nitrogen availability should be the mechanism that drives the downregulation in leaf nitrogen content and photosynthetic capacity under elevated CO_2. This hypothesis has received some support from free air CO_2 enrichment experiments (Reich et al. 2006; Norby et al. 2010), although is not consistently observed across experiments (Finzi et al. 2006; Moore et al. 2006; Liang et al. 2016).

While possible that progressive nitrogen limitation may determine leaf and whole plant acclimation responses to CO_2, growing evidence indicates that leaf nitrogen and photosynthetic capacity are more strongly determined through aboveground growing conditions than by soil resource availability (Dong et al. 2017; Dong et al. 2020; Dong et al. 2022; Smith et al. 2019; Smith and Keenan 2020;

Paillassa et al. 2020; Peng et al. 2021; Querejeta et al. 2022; Westerband et al. 2023), and satellite-derived chlorophyll fluorescence data indicate that increasing atmospheric CO_2 may decrease leaf and canopy demand for nitrogen (Dong et al. 2022). Together, results from these studies suggest that the downregulation in leaf nitrogen content and photosynthetic capacity due to increasing CO_2 may not be as tightly linked to progressive nitrogen limitation as previously hypothesized.

A unification of optimal coordination and photosynthetic least-cost theories predicts that leaves acclimate to elevated CO_2 by downregulating nitrogen allocation to Ribulose-1,5-bisphosphate (RuBP) carboxylase/oxygenase (Rubisco) to optimize resource use efficiencies at the leaf level, which allows for greater resource allocation to whole plant growth (Drake et al. 1997; Wright et al. 2003; Prentice et al. 2014; Smith et al. 2019). The theory predicts that the downregulation in nitrogen allocation to Rubisco results in a stronger downregulation in the maximum rate of Rubisco carboxylation (V_{cmax}) than the maximum rate of RuBP regeneration (J_{max}), which maximizes photosynthetic efficiency by allowing net photosynthesis rates to be equally co-limited by Rubisco carboxylation and RuBP regeneration (Chen et al. 1993; Maire et al. 2012). This acclimation response allows plants to make more efficient use of available light while avoiding overinvestment in Rubisco, which has high nitrogen and energetic costs of building and maintaining (Evans 1989; Evans and Clarke 2019). Instead, additional acquired resources not needed to optimize leaf photosynthesis are allocated to the maintenance of structures that support whole plant growth (e.g., total leaf area, whole plant biomass, etc.) or to allocation processes not related to leaf photosynthesis or growth, such as plant defense mechanisms or leaf structural tissue. Regardless,

optimized resource allocation at the leaf level should allow for greater resource allocation to whole plant growth. The theory indicates that leaf acclimation responses to CO_2 should be independent of changes in soil nitrogen availability. While this leaf acclimation response maximizes nitrogen allocation to structures that support whole plant growth, the theory suggests that the positive effect of elevated CO_2 on whole plant growth may be further stimulated by soil nitrogen availability through a reduction in the cost of acquiring nitrogen (Bae et al. 2015; Perkowski et al. 2021; Lu et al. 2022).

Plants acquire nitrogen by allocating photosynthetically derived carbon belowground in exchange for nitrogen through different nitrogen acquisition strategies. These nitrogen acquisition strategies can include direct uptake pathways such as mass flow or diffusion (Barber 1962), symbioses with mycorrhizal fungi or symbiotic nitrogen-fixing bacteria (Vance and Heichel 1991; Marschner and Dell 1994; Smith and Read 2008; Udvardi and Poole 2013), or through the release of root exudates that prime free-living soil microbial communities (Phillips et al. 2011; Wen et al. 2022). Plants cannot acquire nitrogen without first allocating carbon belowground, which implies an inherent carbon cost to the plant for acquiring nitrogen regardless of nitrogen acquisition strategy. Carbon costs to acquire nitrogen often vary in species with different nitrogen acquisition strategies and are dependent on external environmental factors such as atmospheric CO_2, light availability, and soil nitrogen availability (Brzostek et al. 2014; Terrer et al. 2016; Terrer et al. 2018; Allen et al. 2020; Perkowski et al. 2021; Lu et al. 2022), which suggests that acquisition strategy may be an important factor in determining effects of soil nitrogen availability on leaf and whole plant acclimation responses to

elevated CO_2.

A recent meta-analysis using data across 20 grassland and forest CO_2 enrichment experiments suggested that species which acquire nitrogen from symbiotic nitrogen-fixing bacteria had reduced costs of nitrogen acquisition under elevated CO_2 (Terrer et al. 2018). Findings from this meta-analysis indicated that reductions in costs of nitrogen acquisition in species that form associations with symbiotic nitrogen-fixing bacteria under elevated CO_2 may drive stronger stimulations in whole plant growth and downregulations in V_{cmax} than species that associate with arbuscular mycorrhizal fungi (Smith and Keenan 2020), which generally have higher costs of nitrogen acquisition under elevated CO_2 (Terrer et al. 2018). However, plant investments in symbiotic nitrogen fixation generally decline with increasing nitrogen availability (Dovrat et al. 2018; Perkowski et al. 2021), a response that has been previously inferred to be the result of a shift in the dominant mode of nitrogen acquisition to direct uptake pathways as costs of direct uptake decrease with increasing soil nitrogen availability (Rastetter et al. 2001; Perkowski et al. 2021). Thus, effects of symbiotic nitrogen fixation on plant acclimation responses to CO_2 should decline with increasing soil nitrogen availability, although manipulative experiments that directly test these patterns are rare.

Here, we conducted a 7-week growth chamber experiment using *Glycine max* L. (Merr.) to examine the effects of soil nitrogen fertilization and inoculation with symbiotic nitrogen-fixing bacteria on leaf and whole plant acclimation responses to elevated CO_2. Following patterns expected from theory, we hypothesized that individual leaves should acclimate to elevated CO_2 by more strongly

downregulating V_{cmax} relative to J_{max}, allowing leaf photosynthesis to approach optimal coordination. We expected this response to correspond with a stronger downregulation in leaf nitrogen content than V_{cmax} and J_{max}, which would increase the fraction of leaf nitrogen content allocated to photosynthesis and photosynthetic nitrogen use efficiency. At the whole-plant level, we hypothesized that plants would acclimate to elevated CO_2 by stimulating whole plant growth and productivity, a response that would be driven by a strong positive response of total leaf area and aboveground biomass to elevated CO_2. We predicted that leaf acclimation responses to elevated CO_2 would be independent of soil nitrogen fertilization and inoculation with symbiotic nitrogen-fixing bacteria; however, we expected that increasing soil nitrogen fertilization would increase the positive effect of elevated CO_2 on measures of whole plant growth due to a stronger reduction in the cost of acquiring nitrogen under elevated CO_2 with increasing fertilization. We also expected stronger stimulations in whole plant growth due to inoculation, but that this effect would only be apparent under low fertilization due to a reduction in root nodulation with increasing fertilization.

5.2 Methods

5.2.1 *Seed treatments and experimental design*

Glycine max L. (Merr) seeds were planted in 144 6-liter surface sterilized pots (NS-600, Nursery Supplies, Orange, CA, USA) containing a steam-sterilized 70:30 v:v mix of Sphagnum peat moss (Premier Horticulture, Quakertown, PA, USA) to sand (Pavestone, subsidiary of Quikrete Companies, Atlanta, GA, USA). Before planting, all *G. max* seeds were surface sterilized in 2% sodium hypochlorite

for 3 minutes, followed by three separate 3-minute washes with ultrapure water (MilliQ 7000; MilliporeSigma, Burlington, MA USA). A subset of surface sterilized seeds were inoculated with Bradyrhizobium japonicum (Verdesian N-Dure™ Soybean, Cary, NC, USA) in a slurry following manufacturer recommendations (3.12 g inoculant and 241 g deionized water per 1 kg seed).

Seventy-two pots were randomly planted with surface-sterilized seeds inoculated with *B. japonicum*, while the remaining 72 pots were planted with surface-sterilized uninoculated seeds. Thirty-six pots within each inoculation treatment were randomly placed in one of two atmospheric CO_2 treatments (ambient and 1000 μmol mol^{-1} CO_2). Pots within each unique inoculation-by-CO_2 treatment combination randomly received one of nine soil nitrogen fertilization treatments equivalent to 0, 35, 70, 105, 140, 210, 280, 350, or 630 ppm N. Nitrogen fertilization treatments were created using a modified Hoagland solution (Hoagland and Arnon 1950) designed to keep concentrations of other macronutrients and micronutrients equivalent across treatments (Table S1). Pots received the same fertilization treatment throughout the entire duration experiment, which were applied twice per week in 150 mL doses as topical agents to the soil surface throughout the duration of the experiment. This experimental design yielded a fully factorial experiment with four replicates per unique fertilization-by-inoculation-by-CO_2 combination.

5.2.2 *Growth chamber conditions*

Upon experiment initiation, pots were randomly placed in one of six Percival LED-41L2 growth chambers (Percival Scientific Inc., Perry, IA, USA) over

two experimental iterations due to chamber space limitation. two iterations were conducted such that one iteration included all elevated CO_2 pots and the second iteration included all ambient CO_2 pots. Average ($\pm$ SD) CO_2 concentrations across chambers throughout the experiment were 439 $\pm$ 5 μmol mol^{-1} for the ambient CO_2 treatment and 989 $\pm$ 4 μmol mol^{-1} for the elevated CO_2 treatment.

Daytime growing conditions were simulated using a 16-hour photoperiod, with incoming light radiation set to chamber maximum (mean $\pm$ SD: 1240 $\pm$ 32 μmol m^{-2} s^{-1} across chambers), air temperature set to 25°C, and relative humidity set to 50%. The remaining 8 hours simulated nighttime growing conditions, with incoming light radiation set to 0 μmol m^{-2} s^{-1}, chamber temperature set to 17°C, and relative humidity set to 50%. Transitions between daytime and nighttime growing conditions were simulated by ramping incoming light radiation in 45-minute increments and temperature in 90-minute increments over a 3-hour period (Table S2).

Including the two, 3-hour ramping periods, pots grew under average ($\pm$ SD) daytime light intensity of 1049 $\pm$ 27 μmol m^{-2} s^{-1}. In the elevated CO_2 iteration, pots grew under 24.0 $\pm$ 0.2°C during the day, 16.4 $\pm$ 0.8°C during the night, and 51.6 $\pm$ 0.4% relative humidity. In the ambient CO_2 iteration, pots grew under 23.9 $\pm$ 0.2°C during the day, 16.0 $\pm$ 1.4°C during the night, and 50.3 $\pm$ 0.2% relative humidity. We accounted for climatic differences across the six chambers by shuffling the same group of pots daily throughout the growth chambers. This process was done by iteratively moving the group of pots on the top rack of a chamber to the bottom rack of the same chamber, while simultaneously moving the group of pots on the bottom rack of a chamber to the top rack of the adjacent

chamber. We moved pots within and across chambers every day throughout the course of each experiment iteration.

5.2.3 *Leaf gas exchange measurements*

Gas exchange measurements were collected for all individuals on the seventh week of development. All gas exchange measurements were collected on the center leaf of the most recent fully expanded trifoliate leaf set. Specifically, we measured net photosynthesis (A_{net}; μmol m^{-2} s^{-1}), stomatal conductance (g_{sw}; mol m^{-2} s^{-1}), and intercellular CO_2 (C_{i}; μmol mol^{-1}) concentrations across a range of atmospheric CO_2 concentrations (i.e., an $A_{\text{net}}/C_{\text{i}}$ curve) using the Dynamic Assimilation Technique™. The Dynamic Assimilation Technique™ has been shown to correspond well with traditional steady-state CO_2 response curves in *G. max* (Saathoff and Welles 2021). $A_{\text{net}}/C_{\text{i}}$ curves were generated along a reference CO_2 ramp down from 420 μmol mol^{-1} CO_2 to 20 μmol mol^{-1} CO_2, followed by a ramp up from 420 μmol mol^{-1} CO_2 to 1620 μmol mol^{-1} CO_2 after a 90-second wait period at 420 μmol mol^{-1} CO_2. The ramp rate for each curve was set to 200 μmol mol^{-1} min^{1}, logging every five seconds, which generated 96 data points per response curve. All $A_{\text{net}}/C_{\text{i}}$ curves were generated after A_{net} and g_{sw} stabilized in a LI-6800 cuvette set to a 500 mol s^{-1}, 10,000 rpm mixing fan speed, 1.5 kPa vapor pressure deficit, 25°C leaf temperature, 2000 μmol m^{-2} s^{-1} incoming light radiation, and initial reference CO_2 set to 420 μmol mol^{-1}.

With the same focal leaf used to generate $A_{\text{net}}/C_{\text{i}}$ curves, we measured dark respiration (R_{d25}; μmol m^{-2} s^{-1}) following at least a 30-minute period of darkness. Measurements were collected on a 5-second log interval for 60 seconds

after stabilizing in a LI-6800 cuvette set to a 500 mol s^{-1}, 10,000 rpm mixing fan speed, 1.5 kPa vapor pressure deficit, 25°C leaf temperature, and 420 μmol mol^{-1} reference CO_2 concentration (for both CO^2 concentrations), with incoming light radiation set to 0 μmol m^{-2} s^{-1}. A single dark respiration value was determined for each focal leaf by calculating the mean dark respiration value (i.e. the absolute value of A_{net} during the logging period) across the logging interval.

5.2.4 *Leaf trait measurements*

The focal leaf used to generate $A_{\text{net}}/C_{\text{i}}$ curves and dark respiration was harvested immediately following gas exchange measurements. Images of each focal leaf were curated using a flat-bed scanner to determine wet leaf area using the 'LeafArea' R package (Katabuchi 2015), which automates leaf area calculations using ImageJ software (Schneider et al. 2012). Each leaf was dried at 65°C for at least 48 hours, and subsequently weighed and ground until homogenized. Leaf mass per area (M_{area}; g m^{-2}) was calculated as the ratio of dry leaf biomass to fresh leaf area. Using subsamples of ground and homogenized leaf tissue, we measured leaf nitrogen content (N_{mass}; gN g^{-1}) through elemental combustion analysis (Costech-4010, Costech, Inc., Valencia, CA, USA). Leaf nitrogen content per unit leaf area (N_{area}; gN m^{-2}) was calculated by multiplying N_{mass} and M_{area}.

We extracted chlorophyll content from a second leaf in the same trifoliate leaf set as the focal leaf used to generate $A_{\text{net}}/C_{\text{i}}$ curves. Prior to chlorophyll extraction, we used a cork borer to punch between 3 and 5 0.6 cm^2 disks from the leaf. Separate images of each punched leaf and set of leaf disks were curated using a flat-bed scanner to determine wet leaf area, again quantified using the

'LeafArea' R package (Katabuchi 2015). The punched leaf was dried and weighed after at least 65°C in the drying oven to determine Marea of the chlorophyll leaf.

Leaf disks were shuttled into a test tube containing 10mL dimethyl sulfoxide, vortexed, and incubated at 65degreeC for 120 minutes (Barnes et al. 1992). Incubated test tubes were vortexed again before loaded in 150 μL triplicate aliquots to a 96-well plate. Dimethyl sulfoxide was also loaded in a 150 μL triplicate aliquot as a blank. Absorbance measurements at 649.1 nm ($A_{649.1}$) and 665.1 nm ($A_{665.1}$) were read in each well using a plate reader (Biotek Synergy H1; Biotek Instruments, Winooski, VT USA) (Wellburn 1994), with triplicates subsequently averaged and corrected by the mean of the blank absorbance value. Blank-corrected absorbance values were used to estimate Chl_{a} (μg mL^{-1}) and Chl_{b} (μg mL^{-1}) following equations from Wellburn (1994):

$$Chl_a = 12.47A_{665.1} - 3.62A_{649.1} \tag{5.1}$$

and

$$Chl_b = 25.06A_{665.1} - 6.50A_{649.1} \tag{5.2}$$

Chl_{a} and Chl_{b} were converted to mmol mL^{-1} using the molar mass of chlorophyll a (893.51 g mol^{-1}) and the molar mass of chlorophyll b (907.47 g mol^{-1}), then added together to calculate total chlorophyll content in the dimethyl sulfoxide extractant (mmol mL^{-1}). Total chlorophyll content was multiplied by the volume of the dimethyl sulfoxide extractant (10 mL) and converted to area-based chlorophyll content by dividing by the total area of the leaf disks (Chl_{area}; mmol m^{-2}). Mass-based chlorophyll content (Chl_{mass}; mmol g^{-1}) was calculated by dividing Chl_{area}

by the leaf mass per area of the punched leaf.

5.2.5 *A/C_i curve fitting and parameter estimation*

We fit $A_{\text{net}}/C_{\text{i}}$ curves of each individual using the 'fitaci' function in the 'plantecophys' R package (Duursma 2015). This function estimates the maximum rate of Rubisco carboxylation (V_{cmax}; μmol m^{-2} s^{-1}) and maximum rate of electron transport for RuBP regeneration (J_{max}; μmol m^{-2} s^{-1}) based on the Farquhar biochemical model of C_3 photosynthesis (Farquhar et al. 1980). Triose phosphate utilization (TPU) limitation was included in all curve fits, and all curve fits included measured dark respiration values. As $A_{\text{net}}/C_{\text{i}}$ curves were generated using a common leaf temperature, curves were fit using Michaelis-Menton coefficients for Rubisco affinity to CO_2 (K_{c}; μmol mol^{-1}) and O_2 (K_{o}; μmol mol^{-1}), and the CO_2 compensation point (Γ^*; μmol mol^{-1}) reported in Bernacchi et al. (2001). Specifically, K_{c} was set to 404.9 μmol mol^{-1}, K_{o} was set to 278.4 μmol mol^{-1}, and Γ^* was set to 42.75 μmol mol^{-1}. The use of a common leaf temperature across curves and dark respiration measurements also eliminated the need to manually temperature standardize rate estimates. For clarity, we reference V_{cmax}, J_{max}, and R_{d} estimates throughout the rest of the paper as V_{cmax25}, J_{max25}, and R_{d25}.

5.2.6 Stomatal limitation

We quantified the extent by which stomatal conductance limited photosynthesis (l; unitless) following equations originally described in Farquhar and Sharkey (1982). Stomatal limitation was calculated as:

$$l = 1 - \frac{A_{net}}{A_{mod}} \tag{5.3}$$

where A_{mod} represents the photosynthetic rate where $C_{\mathrm{i}} = C_{\mathrm{a}}$. A_{mod} was calculated as:

$$A_{mod} = V_{cmax25} - \frac{420 - \Gamma^*}{420 + K_m} - R_{d25} \tag{5.4}$$

K_{m} is the Michaelis-Menten coefficient for Rubisco-limited photosynthesis, calculated as:

$$K_m = K_c \cdot \left(1 + \frac{O_i}{K_o}\right) \tag{5.5}$$

where O_{i} refers to leaf intercellular O_2 concentrations, set to 210 μmol mol^{-1}.

5.2.7 *Proportion of leaf nitorgen allocated to photosynthesis and structure*

We used equations from Niinemets and Tenhunen (1997) to estimate the proportion of leaf N content allocated to Rubisco bioenergetics, and light harvesting proteins. The proportion of leaf N allocated to Rubisco (ρ_{rub}; gN gN^{-1}) was calculated as a function of V_{cmax25} and N_{area}:

$$\rho_{rubisco} = \frac{V_{cmax25} N_r}{V_{cr} N_{area}} \tag{5.6}$$

where N_{r} is the amount of nitrogen in Rubisco, set to 0.16 gN (gN in Rubisco)$^{-1}$ and V_{cr} is the maximum rate of RuBP carboxylation per unit Rubisco protein, set to 20.5 μmol CO_2 (g Rubisco)$^{-1}$. The proportion of leaf nitrogen allocated to bioenergetics (ρ_{bioe}; gN gN^{-1}) was similarly calculated as a function of J_{max25} and

1309 N_{area}:

$$\rho_{bioe} = \frac{J_{max25} N_b}{J_{mc} N_{area}} \tag{5.7}$$

1310 where N_{b} is the amount of nitrogen in cytochrome f, set to 0.12407 gN (μmol
1311 cytochrome f)$^{-1}$ assuming a constant 1: 1: 1.2 cytochrome f: ferredoxin NADP
1312 reductase: coupling factor molar ratio (Evans and Seemann 1989; Niinemets and
1313 Tenhunen 1997), and J_{mc} is the capacity of electron transport per cytochrome f,
1314 set to 156 μmol electron (μmol cytochrome f)$^{-1}$s^{-1}.

1315 The proportion of leaf nitrogen allocated to light harvesting proteins was
1316 calculated as a function of Chl_{mass} and N_{mass}:

$$\rho_{light} = \frac{Chl_{mass}}{N_{mass} c_b} \tag{5.8}$$

1317 where c_{b} is the stoichiometry of the light-harvesting chlorophyll complexes of
1318 photosystem II, set to 2.75 mmol chlorophyll (gN in chlorophyll)$^{-1}$. We used the
1319 N_{mass} value of the focal leaf used to generate $A_{\text{net}}/C_{\text{i}}$ curves instead of the leaf
1320 used to extract chlorophyll content, as the two leaves are from the same trifoliate
1321 leaf set and are highly correlated with each other (Figure SX).

1322 The proportion of leaf nitrogen content allocated to photosynthetic tissue
1323 (ρ_{photo}; gN gN^{-1}) was estimated as the sum of ρ_{rubisco}, ρ_{bioe}, and ρ_{light}.

1324 Finally, the proportion of leaf N content allocated to structural tissue (ρ_{str};
1325 gN gN^{-1}) was estimated as:

$$\rho_{structure} = \frac{N_{cw}}{N_{area}} \tag{5.9}$$

where N_{cw} is the leaf N content allocated to cell walls (gN m^{-2}), calculated as a function of M_{area} using an empirical equation from Onoda et al. (2017):

$$N_{cw} = 0.000355 * {M_{area}}^{1.39} \tag{5.10}$$

5.2.8 *Whole plant traits*

Seven weeks after experiment initiation and immediately following gas exchange measurements, we harvested all experimental individuals and separated biomass of each experimental individual into major organ types (leaves, stems, roots, and nodules when present). Fresh leaf area of all harvested leaves was measured using an LI-3100C (Li-COR Biosciences, Lincoln, Nebraska, USA). Total fresh leaf area (cm^2) was calculated as the sum of all leaf areas, including the focal leaf used to collect gas exchange data and the focal leaf used to extract chlorophyll content. All harvested material was dried in an oven set to 65°C for at least 48 hours, weighed, and ground to homogeneity. Leaves and nodules were manually ground either with a mortar and pestle, while stems and roots were ground using a Wiley mill (E3300 Mini Mill; Eberbach Corp., MI, USA). Total dry biomass (g) was calculated as the sum of dry leaf (including focal leaf for both the $A_{\text{net}}/C_{\text{i}}$ curve and leaf used to extract chlorophyll content), stem, root, and root nodule biomass. We also quantified carbon and nitrogen content of each respective organ type through elemental combustion (Costech-4010, Costech, Inc., Valencia, CA, USA) using subsamples of ground and homogenized organ tissue.

Following the approach explained in Perkowski et al. (2021), we calculated structural carbon costs to acquire nitrogen as the ratio of total belowground

carbon biomass to whole plant nitrogen biomass (N_{cost}; gC gN^{-1}). Belowground carbon biomass (C_{bg}; gC) was calculated as the sum of root carbon biomass and root nodule carbon biomass. Root carbon biomass and root nodule carbon biomass was calculated as the product of the organ biomass and the respective organ carbon content. Whole plant nitrogen biomass (N_{wp}; gN) was similarly calculated as the sum of total leaf, stem, root, and root nodule nitrogen biomass, including the focal leaf used for $A_{\text{net}}/C_{\text{i}}$ curve and chlorophyll extractions. Leaf, stem, root, and root nodule nitrogen biomass was calculated as the product of the organ biomass and the respective organ nitrogen content. This calculation only quantifies plant structural carbon costs to acquire nitrogen and does not include any additional costs of nitrogen acquisition associated with respiration, root exudation, or root turnover. An explicit explanation of the limitations for interpreting this calculation can be found in Perkowski et al. (2021) and Terrer et al. (2018).

Finally, plant investments in nitrogen fixation were calculated as the ratio of root nodule biomass to root biomass, where increasing values indicate an increase in plant investments to nitrogen fixation (Dovrat et al. 2018; Dovrat et al. 2020; Perkowski et al. 2021).

5.2.9 *Statistical analyses*

Any uninoculated pots that had substantial root nodule formation (nodule biomass: root biomass values greater than 0.05 g g^{-1}) were removed from our analyses. This was because they were assumed to have been colonized by symbiotic nitrogen-fixing bacteria from outside sources. This decision resulted in the removal

of sixteen pots from our analysis: two pots in the elevated CO_2 treatment that received 35 ppm N, three pots in the elevated CO_2 treatment that received 70 ppm N, one pot in the elevated CO_2 treatment that received 210 ppm N, two pots in the elevated CO_2 treatment that received 280 ppm N, two pots in the ambient CO_2 treatment that received 0 ppm N, three pots in the ambient CO_2 treatment that received 70 ppm N, two pots in the ambient CO_2 treatment that received 105 ppm N, and one pot in the ambient CO_2 treatment that received 280 ppm N.

We built a series of linear mixed effects models to investigate the impacts of CO_2 concentration, soil nitrogen fertilization, and inoculation with *B. japonicum* on *G. max* gas exchange, tradeoffs between nitrogen and water use, whole plant growth, and investment in nitrogen fixation. All models included CO_2 treatment as a categorical fixed effect, inoculation treatment as a categorical fixed effect, soil nitrogen fertilization as a continuous fixed effect, with interaction terms between all three fixed effects. All models also accounted for climatic difference between chambers across experiment iterations by including a random intercept term that nested starting chamber rack by CO_2 treatment. Models with this independent variable structure were created for each of the following dependent variables: N_{area}, M_{area}, N_{mass}, Chl_{area}, V_{cmax25}, J_{max25}, J_{max25}:V_{cmax25}, R_{d25}, g_{sw}, stomatal limitation, ρ_{rubisco}, ρ_{bioe}, ρ_{light}, ρ_{photo}, $\rho_{\text{structure}}$, N_{cost}, C_{bg}, N_{wp}, total biomass, total leaf area, nodule biomass, and the ratio of nodule biomass to root biomass.

We used Shapiro-Wilk tests of normality to determine whether linear mixed effects models satisfied residual normality assumptions. If residual normality assumptions were not met (Shapiro-Wilk: $p < 0.05$), then models were fit using

dependent variables that were natural log transformed. All residual normality assumptions that did not originally satisfy residual normality assumptions were met with either a natural log or square root data transformation (Shapiro-Wilk: $p > 0.05$ in all cases). Specifically, models for N_{area}, N_{mass}, Chl_{area}, V_{cmax25}, J_{max25}, J_{max25}:V_{cmax25}, g_{sw}, stomatal limitation, ρ_{rubisco}, ρ_{bioe}, ρ_{light}, ρ_{photo}, and total leaf area satisfied residual normality assumptions without data transformation. Models for M_{area}, $\rho_{\text{structure}}$, N_{cost}, C_{bg}, N_{wp}, and total biomass satisfied residual normality assumptions with a natural log data transformation, while models for nodule biomass and nodule biomass: root biomass satisfied residual normality assumptions with a square root data transformation.

In all statistical models, we used the 'lmer' function in the 'lme4' R package (Bates et al. 2015) to fit each model and the 'Anova' function in the 'car' R package (Fox and Weisberg 2019) to calculate Type II Wald's χ^2 and determine the significance ($\alpha = 0.05$) of each fixed effect coefficient. We then used the 'emmeans' R package (Lenth 2019) to conduct post-hoc comparisons using Tukey's tests, where degrees of freedom were approximated using the Kenward-Roger approach (Kenward and Roger 1997). All analyses and plots were conducted in R version 4.2.0 (R Core Team 2021).

5.3 Results

5.4 Discussion

Chapter 6

Conclusions

References

Abrams, M. D. and S. A. Mostoller (1995). Gas exchange, leaf structure and nitrogen in contrasting successional tree species growing in open and understory sites during a drought. *Tree Physiology 15*(6), 361–370.

Adams, M. A., T. L. Turnbull, J. I. Sprent, and N. Buchmann (2016). Legumes are different: Leaf nitrogen, photosynthesis, and water use efficiency. *Proceedings of the National Academy of Sciences of the United States of America 113*(15), 4098–4103.

Ainsworth, E. A., P. A. Davey, C. J. Bernacchi, O. C. Dermody, E. A. Heaton, D. J. Moore, P. B. Morgan, S. L. Naidu, H. S. Y. Ra, X. G. Zhu, P. S. Curtis, and S. P. Long (2002). A meta-analysis of elevated [CO_2] effects on soybean (*Glycine max*) physiology, growth and yield. *Global Change Biology 8*(8), 695–709.

Ainsworth, E. A. and S. P. Long (2005). What have we learned from 15 years of free-air CO2 enrichment (FACE)? A meta-analytic review of the responses of photosynthesis, canopy properties and plant production to rising CO_2. *New Phytologist 165*(2), 351–372.

Ainsworth, E. A. and A. Rogers (2007). The response of photosynthesis and stomatal conductance to rising [CO2]: mechanisms and environmental interactions. *Plant, Cell and Environment 30*(3), 258–270.

Allen, K., J. B. Fisher, R. P. Phillips, J. S. Powers, and E. R. Brzostek (2020). Modeling the carbon cost of plant nitrogen and phosphorus uptake across temperate and tropical forests. *Frontiers in Forests and Global Change 3*,

1–12.

Allison, S. D., C. I. Czimczik, and K. K. Treseder (2008). Microbial activity and soil respiration under nitrogen addition in Alaskan boreal forest. *Global Change Biology 14*(5), 1156–1168.

Andersen, M. K., H. Hauggaard-Nielsen, P. Ambus, and E. S. Jensen (2005). Biomass production, symbiotic nitrogen fixation and inorganic N use in dual and tri-component annual intercrops. *Plant and Soil 266*(1-2), 273–287.

Arndal, M. F., A. Tolver, K. S. Larsen, C. Beier, and I. K. Schmidt (2018). Fine root growth and vertical distribution in response to elevated CO2, warming and drought in a mixed heathland–grassland. *Ecosystems 21*(1), 15–30.

Arnone, J. A. (1997). Indices of plant N availability in an alpine grassland under elevated atmospheric CO2. *Plant and Soil 190*(1), 61–66.

Arora, V. K., A. Katavouta, R. G. Williams, C. D. Jones, V. Brovkin, P. Friedlingstein, J. Schwinger, L. Bopp, O. Boucher, P. Cadule, M. A. Chamberlain, J. R. Christian, C. Delire, R. A. Fisher, T. Hajima, T. Ilyina, E. Joetzjer, M. Kawamiya, C. D. Koven, J. P. Krasting, R. M. Law, D. M. Lawrence, A. Lenton, K. Lindsay, J. Pongratz, T. Raddatz, R. Séférian, K. Tachiiri, J. F. Tjiputra, A. Wiltshire, T. Wu, and T. Ziehn (2020). Carbon-concentration and carbon-climate feedbacks in CMIP6 models and their comparison to CMIP5 models. *Biogeosciences 17*(16), 4173–4222.

Bae, K., T. J. Fahey, R. D. Yanai, and M. Fisk (2015). Soil nitrogen availability affects belowground carbon allocation and soil respiration in northern hardwood forests of New Hampshire. *Ecosystems 18*(7), 1179–1191.

Barber, S. A. (1962). A diffusion and mass-flow concept of soil nutrient availability. *Soil Science 93*(1), 39–49.

Barnes, J. D., L. Balaguer, E. Manrique, S. Elvira, and A. W. Davison (1992). A reappraisal of the use of DMSO for the extraction and determination of chlorophylls a and b in lichens and higher plants. *Environmental and Experimental Botany 32*(2), 85–100.

Bates, D., M. Mächler, B. Bolker, and S. Walker (2015). Fitting linear mixed-effects models using lme4. *Journal of Statistical Software 67*(1), 1–48.

Bengtson, P., J. Barker, and S. J. Grayston (2012). Evidence of a strong coupling between root exudation, C and N availability, and stimulated SOM decomposition caused by rhizosphere priming effects. *Ecology and Evolution 2*(8), 1843–1852.

Bernacchi, C. J., E. L. Singsaas, C. Pimentel, A. R. Portis, and S. P. Long (2001). Improved temperature response functions for models of Rubisco-limited photosynthesis. *Plant, Cell and Environment 24*(2), 253–259.

Bialic-Murphy, L., N. G. Smith, P. Voothuluru, R. M. McElderry, M. D. Roche, S. T. Cassidy, S. N. Kivlin, and S. Kalisz (2021). Invasion-induced root–fungal disruptions alter plant water and nitrogen economies. *Ecology Letters 24*(6), 1145–1156.

Bloom, A. J., F. S. Chapin, and H. A. Mooney (1985). Resource limitation in plants - an economic analogy. *Annual Review of Ecology and Systematics 16*(1), 363–392.

Bonan, G. B., M. D. Hartman, W. J. Parton, and W. R. Wieder (2013). Evaluat-

ing litter decomposition in earth system models with long-term litterbag experiments: an example using the Community Land Model version 4 (CLM4). *Global Change Biology 19*(3), 957–974.

Bonan, G. B., P. J. Lawrence, K. W. Oleson, S. Levis, M. Jung, M. Reichstein, D. M. Lawrence, and S. C. Swenson (2011). Improving canopy processes in the Community Land Model version 4 (CLM4) using global flux fields empirically inferred from FLUXNET data. *Journal of Geophysical Research 116*(G2), G02014.

Booth, B. B. B., C. D. Jones, M. Collins, I. J. Totterdell, P. M. Cox, S. Sitch, C. Huntingford, R. A. Betts, G. R. Harris, and J. Lloyd (2012). High sensitivity of future global warming to land carbon cycle processes. *Environmental Research Letters 7*(2), 024002.

Borer, E. T., W. S. Harpole, P. B. Adler, E. M. Lind, J. L. Orrock, E. W. Seabloom, and M. D. Smith (2014). Finding generality in ecology: A model for globally distributed experiments. *Methods in Ecology and Evolution 5*(1), 65–73.

Braghiere, R. K., J. B. Fisher, K. Allen, E. Brzostek, M. Shi, X. Yang, D. M. Ricciuto, R. A. Fisher, Q. Zhu, and R. P. Phillips (2022). Modeling global carbon costs of plant nitrogen and phosphorus acquisition. *Journal of Advances in Modeling Earth Systems 14*(8), 1–23.

Brix, H. (1971). Effects of nitrogen fertilization on photosynthesis and respiration in Douglas-fir. *Forest Science 17*(4), 407–414.

Brzostek, E. R., J. B. Fisher, and R. P. Phillips (2014). Modeling the carbon cost of plant nitrogen acquisition: Mycorrhizal trade-offs and multipath

resistance uptake improve predictions of retranslocation. *Journal of Geophysical Research: Biogeosciences 119*, 1684–1697.

Bubier, J. L., R. Smith, S. Juutinen, T. R. Moore, R. Minocha, S. Long, and S. Minocha (2011). Effects of nutrient addition on leaf chemistry, morphology, and photosynthetic capacity of three bog shrubs. *Oecologia 167*(2), 355–368.

Cernusak, L. A., N. Ubierna, K. Winter, J. A. M. Holtum, J. D. Marshall, and G. D. Farquhar (2013). Environmental and physiological determinants of carbon isotope discrimination in terrestrial plants. *New Phytologist 200*(4), 950–965.

Chen, J.-L., J. F. Reynolds, P. C. Harley, and J. D. Tenhunen (1993). Coordination theory of leaf nitrogen distribution in a canopy. *Oecologia 93*(1), 63–69.

Clark, D. B., L. M. Mercado, S. Sitch, C. D. Jones, N. Gedney, M. J. Best, M. Pryor, G. G. Rooney, R. L. H. Essery, E. Blyth, O. Boucher, R. J. Harding, C. Huntingford, and P. M. Cox (2011). The Joint UK Land Environment Simulator (JULES), model description. Part 2: Carbon fluxes and vegetation dynamics. *Geoscientific Model Development 4*(3), 701–722.

Cornwell, W. K., J. H. C. Cornelissen, K. Amatangelo, E. Dorrepaal, V. T. Eviner, O. Godoy, S. E. Hobbie, B. Hoorens, H. Kurokawa, N. Pérez-Harguindeguy, H. M. Quested, L. S. Santiago, D. A. Wardle, I. J. Wright, R. Aerts, S. D. Allison, P. van Bodegom, V. Brovkin, A. Chatain, T. V. Callaghan, S. Díaz, E. Garnier, D. E. Gurvich, E. Kazakou, J. A. Klein, J. Read, P. B. Reich, N. A. Soudzilovskaia, M. V. Vaieretti, and M. Westoby

(2008). Plant species traits are the predominant control on litter decomposition rates within biomes worldwide. *Ecology Letters 11*(10), 1065–1071.

Cornwell, W. K., I. J. Wright, J. Turner, V. Maire, M. M. Barbour, L. A. Cernusak, T. E. Dawson, D. S. Ellsworth, G. D. Farquhar, H. Griffiths, C. Keitel, A. Knohl, P. B. Reich, D. G. Williams, R. Bhaskar, J. H. C. Cornelissen, A. Richards, S. Schmidt, F. Valladares, C. Körner, E.-D. Schulze, N. Buchmann, and L. S. Santiago (2018). Climate and soils together regulate photosynthetic carbon isotope discrimination within C_3 plants worldwide. *Global Ecology and Biogeography 27*(9), 1056–1067.

Curtis, P. S. (1996). A meta-analysis of leaf gas exchange and nitrogen in trees grown under elevated carbon dioxide. *Plant, Cell and Environment 19*(2), 127–137.

Davies-Barnard, T., J. Meyerholt, S. Zaehle, P. Friedlingstein, V. Brovkin, Y. Fan, R. A. Fisher, C. D. Jones, H. Lee, D. Peano, B. Smith, D. Wårlind, and A. J. Wiltshire (2020). Nitrogen cycling in CMIP6 land surface models: progress and limitations. *Biogeosciences 17*(20), 5129–5148.

Delaire, M., E. Frak, M. Sigogne, B. Adam, F. Beaujard, and X. Le Roux (2005). Sudden increase in atmospheric CO_2 concentration reveals strong coupling between shoot carbon uptake and root nutrient uptake in young walnut trees. *Tree Physiology 25*(2), 229–235.

Doane, T. A. and W. R. Horwáth (2003). Spectrophotometric determination of nitrate with a single reagent. *Analytical Letters 36*(12), 2713–2722.

Dong, N., I. C. Prentice, B. J. Evans, S. Caddy-Retalic, A. J. Lowe, and I. J. Wright (2017). Leaf nitrogen from first principles: field evidence for adaptive

variation with climate. *Biogeosciences 14*(2), 481–495.

Dong, N., I. C. Prentice, I. J. Wright, B. J. Evans, H. F. Togashi, S. Caddy-Retalic, F. A. McInerney, B. Sparrow, E. Leitch, and A. J. Lowe (2020). Components of leaf-trait variation along environmental gradients. *New Phytologist 228*(1), 82–94.

Dong, N., I. C. Prentice, I. J. Wright, H. Wang, O. K. Atkin, K. J. Bloomfield, T. F. Domingues, S. M. Gleason, V. Maire, Y. Onoda, H. Poorter, and N. G. Smith (2022). Leaf nitrogen from the perspective of optimal plant function. *Journal of Ecology 110*(11), 2585–2602.

Dong, N., I. J. Wright, J. M. Chen, X. Luo, H. Wang, T. F. Keenan, N. G. Smith, and I. C. Prentice (2022). Rising CO_2 and warming reduce global canopy demand for nitrogen. *New Phytologist 235*(5), 1692–1700.

Dovrat, G., H. Bakhshian, T. Masci, and E. Sheffer (2020). The nitrogen economic spectrum of legume stoichiometry and fixation strategy. *New Phytologist 227*(2), 365–375.

Dovrat, G., T. Masci, H. Bakhshian, E. Mayzlish Gati, S. Golan, and E. Sheffer (2018). Drought-adapted plants dramatically downregulate dinitrogen fixation: Evidences from Mediterranean legume shrubs. *Journal of Ecology 106*(4), 1534–1544.

Drake, B. G., M. A. Gonzàlez-Meler, and S. P. Long (1997). More efficient plants: a consequence of rising atmospheric CO_2? *Annual Review of Plant Biology 48*, 609–639.

Duursma, R. A. (2015). Plantecophys - An R Package for Analysing and Mod-

elling Leaf Gas Exchange Data. *PLOS ONE 10*(11), e0143346.

Eastman, B. A., M. B. Adams, E. R. Brzostek, M. B. Burnham, J. E. Carrara, C. Kelly, B. E. McNeil, C. A. Walter, and W. T. Peterjohn (2021). Altered plant carbon partitioning enhanced forest ecosystem carbon storage after 25 years of nitrogen additions. *New Phytologist 230*(4), 1435–1448.

Ellsworth, D. S. and P. B. Reich (1996). Photosynthesis and leaf nitrogen in five Amazonian tree species during early secondary succession. *Ecology 77*(2), 581–594.

Espelta, J. M., P. Cortés, M. Mangirón, and J. Retana (2005). Differences in biomass partitioning, leaf nitrogen content, and water use efficiency d13C result in similar performance of seedlings of two Mediterranean oaks with contrasting leaf habit. *Ecoscience 12*(4), 447–454.

Evans, J. R. (1989). Photosynthesis and nitrogen relationships in leaves of C_3 plants. *Oecologia 78*(1), 9–19.

Evans, J. R. and V. C. Clarke (2019). The nitrogen cost of photosynthesis. *Journal of Experimental Botany 70*(1), 7–15.

Evans, J. R. and H. Poorter (2001). Photosynthetic acclimation of plants to growth irradiance: the relative importance of specific leaf area and nitrogen partitioning in maximizing carbon gain. *Plant, Cell and Environment 24*(8), 755–767.

Evans, J. R. and J. R. Seemann (1989). The allocation of protein nitrogen in the photosynthetic apparatus: costs, consequences, and control. *Photosynthesis 8*, 183–205.

Exbrayat, J.-F., A. A. Bloom, P. Falloon, A. Ito, T. L. Smallman, and M. Williams (2018). Reliability ensemble averaging of 21^{st} century projections of terrestrial net primary productivity reduces global and regional uncertainties. *Earth System Dynamics 9*(1), 153–165.

Farquhar, G. D., J. R. Ehleringer, and K. T. Hubick (1989). Carbon Isotope Discrimination and Photosynthesis. *Annual Review of Plant Physiology and Plant Molecular Biology 40*(1), 503–537.

Farquhar, G. D. and T. D. Sharkey (1982). Stomatal conductance and photosynthesis. *Annual Review of Plant Physiology 33*(1), 317–345.

Farquhar, G. D., S. von Caemmerer, and J. A. Berry (1980). A biochemical model of photosynthetic CO2 assimilation in leaves of C3 species. *Planta 149*(1), 78–90.

Fay, P. A., S. M. Prober, W. S. Harpole, J. M. H. Knops, J. D. Bakker, E. T. Borer, E. M. Lind, A. S. MacDougall, E. W. Seabloom, P. D. Wragg, P. B. Adler, D. M. Blumenthal, Y. M. Buckley, C. Chu, E. E. Cleland, S. L. Collins, K. F. Davies, G. Du, X. Feng, J. Firn, D. S. Gruner, N. Hagenah, Y. Hautier, R. W. Heckman, V. L. Jin, K. P. Kirkman, J. A. Klein, L. M. Ladwig, Q. Li, R. L. McCulley, B. A. Melbourne, C. E. Mitchell, J. L. Moore, J. W. Morgan, A. C. Risch, M. Schütz, C. J. Stevens, D. A. Wedin, and L. H. Yang (2015). Grassland productivity limited by multiple nutrients. *Nature Plants 1*(7), 15080.

Field, C. B. and H. A. Mooney (1986). The photosynthesis-nitrogen relationship in wild plants. In T. J. Givnish (Ed.), *On the Economy of Plant Form and Function*, pp. 25–55. Cambridge: Cambridge University Press.

Finzi, A. C., D. J. P. Moore, E. H. DeLucia, J. Lichter, K. S. Hofmockel, R. B. Jackson, H. S. Kim, R. Matamala, H. R. McCarthy, R. Oren, J. S. Pippen, and W. H. Schlesinger (2006). Progressive nitrogen limitation of ecosystem processes under elevated CO2 in a warm-temperate forest. *Ecology 87*(1), 15–25.

Firn, J., J. M. McGree, E. Harvey, H. Flores Moreno, M. Schutz, Y. M. Buckley, E. T. Borer, E. W. Seabloom, K. J. La Pierre, A. M. MacDougall, S. M. Prober, C. J. Stevens, L. L. Sullivan, E. Porter, E. Ladouceur, C. Allen, K. H. Moromizato, J. W. Morgan, W. S. Harpole, Y. Hautier, N. Eisenhauer, J. P. Wright, P. B. Adler, C. A. Arnillas, J. D. Bakker, L. Biederman, A. A. D. Broadbent, C. S. Brown, M. N. Bugalho, M. C. Caldeira, E. E. Cleland, A. Ebeling, P. A. Fay, N. Hagenah, A. R. Kleinhesselink, R. Mitchell, J. L. Moore, C. Nogueira, P. L. Peri, C. Roscher, M. D. Smith, P. D. Wragg, and A. C. Risch (2019). Leaf nutrients, not specific leaf area, are consistent indicators of elevated nutrient inputs. *Nature Ecology and Evolution 3*(3), 400–406.

Fisher, J. B., S. Sitch, Y. Malhi, R. A. Fisher, C. Huntingford, and S.-Y. Tan (2010). Carbon cost of plant nitrogen acquisition: A mechanistic, globally applicable model of plant nitrogen uptake, retranslocation, and fixation. *Global Biogeochemical Cycles 24*(1), 1–17.

Fox, J. and S. Weisberg (2019). *An R companion to applied regression* (Third edit ed.). Thousand Oaks, California: Sage.

Franklin, O., R. E. McMurtrie, C. M. Iversen, K. Y. Crous, A. C. Finzi, D. Tissue, D. S. Ellsworth, R. Oren, and R. J. Norby (2009). Forest fine-root

production and nitrogen use under elevated CO_2: contrasting responses in evergreen and deciduous trees explained by a common principle. *Global Change Biology 15*(1), 132–144.

Friedlingstein, P., M. Meinshausen, V. K. Arora, C. D. Jones, A. Anav, S. K. Liddicoat, and R. Knutti (2014). Uncertainties in CMIP5 climate projections due to carbon cycle feedbacks. *Journal of Climate 27*(2), 511–526.

Friel, C. A. and M. L. Friesen (2019). Legumes modulate allocation to rhizobial nitrogen fixation in response to factorial light and nitrogen manipulation. *Frontiers in Plant Science 10*, 1316.

Fujikake, H., A. Yamazaki, N. Ohtake, K. Sueoshi, S. Matsuhashi, T. Ito, C. Mizuniwa, T. Kume, S. Hoshimoto, N.-S. Ishioka, S. Watanabe, A. Osa, T. Sekine, H. Uchida, A. Tsuji, and T. Ohyama (2003). Quick and reversible inhibition of soybean root nodule growth by nitrate involves a decrease in sucrose supply to nodules. *Journal of Experimental Botany 54*(386), 1379–1388.

Ghimire, B., W. J. Riley, C. D. Koven, J. Kattge, A. Rogers, P. B. Reich, and I. J. Wright (2017). A global trait-based approach to estimate leaf nitrogen functional allocation from observations:. *Ecological Applications 27*(5), 1421–1434.

Giardina, C. P., M. D. Coleman, J. E. Hancock, J. S. King, E. A. Lilleskov, W. M. Loya, K. S. Pregitzer, M. G. Ryan, and C. C. Trettin (2005). The response of belowground carbon allocation in forests to global change. In D. Binkley and O. Manyailo (Eds.), *Tree Species Effects on Soils: Implications for Global Change* (Volume 55 ed.)., Chapter Chapter 7, pp. 119–154.

Berlin/Heidelberg: Springer-Verlag.

Gibson, A. H. and J. E. Harper (1985). Nitrate effect on nodulation of soybean by *Bradyrhizobium japonicum*. *Crop Science 25*(3), 497–501.

Gill, A. L. and A. C. Finzi (2016). Belowground carbon flux links biogeochemical cycles and resource-use efficiency at the global scale. *Ecology Letters 19*(12), 1419–1428.

Goll, D. S., V. Brovkin, B. R. Parida, C. H. Reick, J. Kattge, P. B. Reich, P. M. van Bodegom, and Ü. Niinemets (2012). Nutrient limitation reduces land carbon uptake in simulations with a model of combined carbon, nitrogen and phosphorus cycling. *Biogeosciences Discussions 9*(3), 3173–3232.

Gregory, L. M., A. M. McClain, D. M. Kramer, J. D. Pardo, K. E. Smith, O. L. Tessmer, B. J. Walker, L. G. Ziccardi, and T. D. Sharkey (2021, oct). The triose phosphate utilization limitation of photosynthetic rate: Out of global models but important for leaf models. *Plant, Cell and Environment 44*(10), 3223–3226.

Guerrieri, R., M. Mencuccini, L. J. Sheppard, M. Saurer, M. P. Perks, P. Levy, M. A. Sutton, M. Borghetti, and J. Grace (2011). The legacy of enhanced N and S deposition as revealed by the combined analysis of δ13C, δ18O and δ15N in tree rings. *Global Change Biology 17*(5), 1946–1962.

Gulmon, S. L. and C. C. Chu (1981). The effects of light and nitrogen on photosynthesis, leaf characteristics, and dry matter allocation in the chaparral shrub, Diplacus aurantiacus. *Oecologia 49*(2), 207–212.

Gutschick, V. P. (1981). Evolved strategies in nitrogen acquisition by plants.

The American Naturalist 118(5), 607–637.

Hallik, L., Ü. Niinemets, and I. J. Wright (2009). Are species shade and drought tolerance reflected in leaf-level structural and functional differentiation in Northern Hemisphere temperate woody flora? *New Phytologist 184*(1), 257–274.

Harrison, M. T., E. J. Edwards, G. D. Farquhar, A. B. Nicotra, and J. R. Evans (2009). Nitrogen in cell walls of sclerophyllous leaves accounts for little of the variation in photosynthetic nitrogen-use efficiency. *Plant, Cell and Environment 32*(3), 259–270.

Harrison, S. P., W. Cramer, O. Franklin, I. C. Prentice, H. Wang, Å. Brännström, H. de Boer, U. Dieckmann, J. Joshi, T. F. Keenan, A. Lavergne, S. Manzoni, G. Mengoli, C. Morfopoulos, J. Peñuelas, S. Pietsch, K. T. Rebel, Y. Ryu, N. G. Smith, B. D. Stocker, and I. J. Wright (2021). Eco-evolutionary optimality as a means to improve vegetation and land-surface models. *New Phytologist 231*(6), 2125–2141.

Henneron, L., P. Kardol, D. A. Wardle, C. Cros, and S. Fontaine (2020). Rhizosphere control of soil nitrogen cycling: a key component of plant economic strategies. *New Phytologist 228*(4), 1269–1282.

Hikosaka, K. and A. Shigeno (2009). The role of Rubisco and cell walls in the interspecific variation in photosynthetic capacity. *Oecologia 160*(3), 443–451.

Hoagland, D. R. and D. I. Arnon (1950). The water culture method for growing plants without soil. *California Agricultural Experiment Station: 347 347*(2), 1–32.

1722 Hobbie, E. A. (2006). Carbon allocation to ectomycorrhizal fungi correlates
1723 with belowground allocation in culture studies. *Ecology 87*(3), 563–569.

1724 Hobbie, E. A. and J. E. Hobbie (2008). Natural abundance of ^{15}N in nitrogen-
1725 limited forests and tundra can estimate nitrogen cycling through mycorrhizal
1726 fungi: a review. *Ecosystems 11*(5), 815–830.

1727 Hoek, T. A., K. Axelrod, T. Biancalani, E. A. Yurtsev, J. Liu, and J. Gore
1728 (2016). Resource availability modulates the cooperative and competitive na-
1729 ture of a microbial cross-feeding mutualism. *PLOS Biology 14*(8), e1002540.

1730 Högberg, M. N., M. J. I. Briones, S. G. Keel, D. B. Metcalfe, C. Campbell, A. J.
1731 Midwood, B. Thornton, V. Hurry, S. Linder, T. Näsholm, and P. Högberg
1732 (2010). Quantification of effects of season and nitrogen supply on tree below-
1733 ground carbon transfer to ectomycorrhizal fungi and other soil organisms in
1734 a boreal pine forest. *New Phytologist 187*(2), 485–493.

1735 Högberg, P., M. N. Högberg, S. G. Göttlicher, N. R. Betson, S. G. Keel, D. B.
1736 Metcalfe, C. Campbell, A. Schindlbacher, V. Hurry, T. Lundmark, S. Linder,
1737 and T. Näsholm (2008). High temporal resolution tracing of photosynthate
1738 carbon from the tree canopy to forest soil microorganisms. *New Phytolo-*
1739 *gist 177*(1), 220–228.

1740 Houlton, B. Z., Y.-P. Wang, P. M. Vitousek, and C. B. Field (2008). A uni-
1741 fying framework for dinitrogen fixation in the terrestrial biosphere. *Na-*
1742 *ture 454*(7202), 327–330.

1743 Hungate, B. A., J. S. Dukes, M. R. Shaw, Y. Luo, and C. B. Field (2003).
1744 Nitrogen and climate change. *Science 302*(5650), 1512–1513.

IPCC (2021). *Climate Change 2021: The Physical Science Basis. Contribution of Working Group I to the Sixth Assessment Report of the Intergovernmental Panel on Climate Change*. Cambridge University Press.

Johnson, N. C., J. H. Graham, and F. A. Smith (1997). Functioning of mycorrhizal associations along the mutualism-parasitism continuum. *New Phytologist 135*(4), 575–585.

Kaiser, C., M. R. Kilburn, P. L. Clode, L. Fuchslueger, M. Koranda, J. B. Cliff, Z. M. Solaiman, and D. V. Murphy (2015). Exploring the transfer of recent plant photosynthates to soil microbes: mycorrhizal pathway vs direct root exudation. *New Phytologist 205*(4), 1537–1551.

Katabuchi, M. (2015). LeafArea: An R package for rapid digital analysis of leaf area. *Ecological Research 30*(6), 1073–1077.

Kattge, J. and W. Knorr (2007). Temperature acclimation in a biochemical model of photosynthesis: a reanalysis of data from 36 species. *Plant, Cell and Environment 30*(9), 1176–1190.

Kattge, J., W. Knorr, T. Raddatz, and C. Wirth (2009). Quantifying photosynthetic capacity and its relationship to leaf nitrogen content for global-scale terrestrial biosphere models. *Global Change Biology 15*(4), 976–991.

Kayler, Z., A. Gessler, and N. Buchmann (2010). What is the speed of link between aboveground and belowground processes? *New Phytologist 187*(4), 885–888.

Kayler, Z., C. Keitel, K. Jansen, and A. Gessler (2017). Experimental evidence of two mechanisms coupling leaf-level C assimilation to rhizosphere

CO₂ release. *Environmental and Experimental Botany 135*, 21–26.

Keeling, C. D., W. G. Mook, and P. P. Tans (1979, jan). Recent trends in the ¹³C/¹²C ratio of atmospheric carbon dioxide. *Nature 277*(5692), 121–123.

Kenward, M. G. and J. H. Roger (1997). Small sample inference for fixed effects from restricted maximum likelihood. *Biometrics 53*(3), 983.

Knapp, A. K., M. L. Avolio, C. Beier, C. J. W. Carroll, S. L. Collins, J. S. Dukes, L. H. Fraser, R. J. Griffin-Nolan, D. L. Hoover, A. Jentsch, M. E. Loik, R. P. Phillips, A. K. Post, O. E. Sala, I. J. Slette, L. Yahdjian, and M. D. Smith (2017). Pushing precipitation to the extremes in distributed experiments: recommendations for simulating wet and dry years. *Global Change Biology 23*(5), 1774–1782.

Knorr, W. (2000). Annual and interannual CO₂ exchanges of the terrestrial biosphere: process-based simulations and uncertainties. *Global Ecology and Biogeography 9*(3), 225–252.

Knorr, W. and M. Heimann (2001). Uncertainties in global terrestrial biosphere modeling: 1. A comprehensive sensitivity analysis with a new photosynthesis and energy balance scheme. *Global Biogeochemical Cycles 15*(1), 207–225.

Kulmatiski, A., P. B. Adler, J. M. Stark, and A. T. Tredennick (2017). Water and nitrogen uptake are better associated with resource availability than root biomass. *Ecosphere 8*(3), e01738.

Lawrence, D. M., R. A. Fisher, C. D. Koven, K. W. Oleson, S. C. Swen-

son, G. B. Bonan, N. Collier, B. Ghimire, L. Kampenhout, D. Kennedy, E. Kluzek, P. J. Lawrence, F. Li, H. Li, D. L. Lombardozzi, W. J. Riley, W. J. Sacks, M. Shi, M. Vertenstein, W. R. Wieder, C. Xu, A. A. Ali, A. M. Badger, G. Bisht, M. Broeke, M. A. Brunke, S. P. Burns, J. Buzan, M. Clark, A. Craig, K. M. Dahlin, B. Drewniak, J. B. Fisher, M. Flanner, A. M. Fox, P. Gentine, F. M. Hoffman, G. Keppel-Aleks, R. Knox, S. Kumar, J. Lenaerts, L. R. Leung, W. H. Lipscomb, Y. Lu, A. Pandey, J. D. Pelletier, J. Perket, J. T. Randerson, D. M. Ricciuto, B. M. Sanderson, A. Slater, Z. M. Subin, J. Tang, R. Q. Thomas, M. Val Martin, and X. Zeng (2019). The Community Land Model Version 5: description of new features, benchmarking, and impact of forcing uncertainty. *Journal of Advances in Modeling Earth Systems 11*(12), 4245–4287.

LeBauer, D. S. and K. K. Treseder (2008). Nitrogen limitation of net primary productivity. *Ecology 89*(2), 371–379.

Lenth, R. (2019). emmeans: estimated marginal means, aka least-squares means.

Li, W., H. Zhang, G. Huang, R. Liu, H. Wu, C. Zhao, and N. G. McDowell (2020). Effects of nitrogen enrichment on tree carbon allocation: A global synthesis. *Global Ecology and Biogeography 29*(3), 573–589.

Liang, J., X. Qi, L. Souza, and Y. Luo (2016). Processes regulating progressive nitrogen limitation under elevated carbon dioxide: a meta-analysis. *Biogeosciences 13*(9), 2689–2699.

Liang, X., T. Zhang, X. Lu, D. S. Ellsworth, H. BassiriRad, C. You, D. Wang, P. He, Q. Deng, H. Liu, J. Mo, and Q. Ye (2020). Global response patterns of

plant photosynthesis to nitrogen addition: A meta-analysis. *Global Change Biology 26*(6), 3585–3600.

Lu, J., J. Yang, C. Keitel, L. Yin, P. Wang, W. Cheng, and F. A. Dijkstra (2022). Belowground Carbon Efficiency for Nitrogen and Phosphorus Acquisition Varies Between Lolium perenne and Trifolium repens and Depends on Phosphorus Fertilization. *Frontiers in Plant Science 13*, 1–9.

Luo, X., T. F. Keenan, J. M. Chen, H. Croft, I. C. Prentice, N. G. Smith, A. P. Walker, H. Wang, R. Wang, C. Xu, and Y. Zhang (2021). Global variation in the fraction of leaf nitrogen allocated to photosynthesis. *Nature Communications 12*(1), 4866.

Luo, Y., W. S. Currie, J. S. Dukes, A. C. Finzi, U. A. Hartwig, B. A. Hungate, R. E. McMurtrie, R. Oren, W. J. Parton, D. E. Pataki, R. M. Shaw, D. R. Zak, and C. B. Field (2004). Progressive nitrogen limitation of ecosystem responses to rising atmospheric carbon dioxide. *BioScience 54*(8), 731–739.

Maire, V., P. Martre, J. Kattge, F. Gastal, G. Esser, S. Fontaine, and J.-F. Soussana (2012). The coordination of leaf photosynthesis links C and N fluxes in C_3 plant species. *PLoS ONE 7*(6), e38345.

Makino, A. (2003). Rubisco and nitrogen relationships in rice: leaf photosynthesis and plant growth. *Soil Science and Plant Nutrition 49*(3), 319–327.

Markham, J. H. and C. Zekveld (2007). Nitrogen fixation makes biomass allocation to roots independent of soil nitrogen supply. *Canadian Journal of Botany* (9), 787–793.

Marschner, H. and B. Dell (1994). Nutrient uptake in mycorrhizal symbiosis.

Plant and Soil 159(1), 89–102.

Matamala, R. and W. H. Schlesinger (2000). Effects of elevated atmospheric CO₂ on fine root production and activity in an intact temperate forest ecosystem. *Global Change Biology 6*(8), 967–979.

Medlyn, B. E., E. Dreyer, D. S. Ellsworth, M. Forstreuter, P. C. Harley, M. U. F. Kirschbaum, X. Le Roux, P. Montpied, J. Strassemeyer, A. Walcroft, K. Wang, and D. Loustau (2002). Temperature response of parameters of a biochemically based model of photosynthesis. II. A review of experimental data. *Plant, Cell and Environment 25*(9), 1167–1179.

Menge, D. N. L., S. A. Levin, and L. O. Hedin (2008). Evolutionary tradeoffs can select against nitrogen fixation and thereby maintain nitrogen limitation. *Proceedings of the National Academy of Sciences 105*(5), 1573–1578.

Menne, M. J., I. Durre, R. S. Vose, B. E. Gleason, and T. G. Houston (2012). An overview of the global historical climatology network-daily database. *Journal of Atmospheric and Oceanic Technology 29*(7), 897–910.

Meyerholt, J., K. Sickel, and S. Zaehle (2020). Ensemble projections elucidate effects of uncertainty in terrestrial nitrogen limitation on future carbon uptake. *Global Change Biology 26*(7), 3978–3996.

Meyerholt, J., S. Zaehle, and M. J. Smith (2016). Variability of projected terrestrial biosphere responses to elevated levels of atmospheric CO₂ due to uncertainty in biological nitrogen fixation. *Biogeosciences 13*(5), 1491–1518.

Minocha, R., S. Long, A. H. Magill, J. D. Aber, and W. H. McDowell (2000).

Foliar free polyamine and inorganic ion content in relation to soil and soil solution chemistry in two fertilized forest stands at the Harvard Forest, Massachusetts. *Plant and Soil 222*(1-2), 119–137.

Moore, D. J., S. Aref, R. M. Ho, J. S. Pippen, J. G. Hamilton, and E. H. De Lucia (2006). Annual basal area increment and growth duration of Pinus taeda in response to eight years of free-air carbon dioxide enrichment. *Global Change Biology 12*(8), 1367–1377.

Morgan, J. A., D. E. Pataki, C. Körner, H. Clark, S. J. Del Grosso, J. M. Grünzweig, A. K. Knapp, A. R. Mosier, P. C. D. Newton, P. A. Niklaus, J. B. Nippert, R. S. Nowak, W. J. Parton, H. W. Polley, and M. R. Shaw (2004). Water relations in grassland and desert ecosystems exposed to elevated atmospheric CO_2. *Oecologia 140*(1), 11–25.

Muñoz, N., X. Qi, M. W. Li, M. Xie, Y. Gao, M. Y. Cheung, F. L. Wong, and H.-M. Lam (2016). Improvement in nitrogen fixation capacity could be part of the domestication process in soybean. *Heredity 117*(2), 84–93.

Nadelhoffer, K. J. and J. W. Raich (1992). Fine root production estimates and belowground carbon allocation in forest ecosystems. *Ecology 73*(4), 1139–1147.

Niinemets, Ü. and J. D. Tenhunen (1997). A model separating leaf structural and physiological effects on carbon gain along light gradients for the shade-tolerant species Acer saccharum. *Plant, Cell and Environment 20*(7), 845–866.

Norby, R. J., J. Ledford, C. D. Reilly, N. E. Miller, and E. G. O'Neill (2004). Fine-root production dominates response of a deciduous forest to

atmospheric CO2 enrichment. *Proceedings of the National Academy of Sciences 101*(26), 9689–9693.

Norby, R. J., J. M. Warren, C. M. Iversen, B. E. Medlyn, and R. E. McMurtrie (2010). CO_2 enhancement of forest productivity constrained by limited nitrogen availability. *Proceedings of the National Academy of Sciences 107*(45), 19368–19373.

Noyce, G. L., M. L. Kirwan, R. L. Rich, and J. P. Megonigal (2019). Asynchronous nitrogen supply and demand produce nonlinear plant allocation responses to warming and elevated CO₂. *Proceedings of the National Academy of Sciences 116*(43), 21623–21628.

Onoda, Y., K. Hikosaka, and T. Hirose (2004). Allocation of nitrogen to cell walls decreases photosynthetic nitrogen-use efficiency. *Functional Ecology 18*(3), 419–425.

Onoda, Y., I. J. Wright, J. R. Evans, K. Hikosaka, K. Kitajima, Ü. Niinemets, H. Poorter, T. Tosens, and M. Westoby (2017). Physiological and structural tradeoffs underlying the leaf economics spectrum. *New Phytologist 214*(4), 1447–1463.

Paillassa, J., I. J. Wright, I. C. Prentice, S. Pepin, N. G. Smith, G. Ethier, A. C. Westerband, L. J. Lamarque, H. Wang, W. K. Cornwell, and V. Maire (2020). When and where soil is important to modify the carbon and water economy of leaves. *New Phytologist 228*(1), 121–135.

Parvin, S., S. Uddin, S. Tausz Posch, R. Armstrong, and M. Tausz (2020). Carbon sink strength of nodules but not other organs modulates photosynthesis of faba bean (*i>Vicia faba</i>*) grown under elevated [CO_2] and different

water supply. *New Phytologist 227*(1), 132–145.

Peng, Y., K. J. Bloomfield, L. A. Cernusak, T. F. Domingues, and I. C. Prentice (2021). Global climate and nutrient controls of photosynthetic capacity. *Communications Biology 4*(1), 462.

Perkowski, E. A., E. F. Waring, and N. G. Smith (2021). Root mass carbon costs to acquire nitrogen are determined by nitrogen and light availability in two species with different nitrogen acquisition strategies. *Journal of Experimental Botany 72*(15), 5766–5776.

Phillips, R. P., E. R. Brzostek, and M. G. Midgley (2013). The mycorrhizal-associated nutrient economy: a new framework for predicting carbon-nutrient couplings in temperate forests. *New Phytologist 199*(1), 41–51.

Phillips, R. P., A. C. Finzi, and E. S. Bernhardt (2011). Enhanced root exudation induces microbial feedbacks to N cycling in a pine forest under long-term CO2 fumigation. *Ecology Letters 14*(2), 187–194.

Pons, T. L. and R. W. Pearcy (1994). Nitrogen reallocation and photosynthetic acclimation in response to partial shading in soybean plants. *Physiologia Plantarum 92*(4), 636–644.

Poorter, H., J. Bühler, D. Van Dusschoten, J. Climent, and J. A. Postma (2012). Pot size matters: A meta-analysis of the effects of rooting volume on plant growth. *Functional Plant Biology 39*(11), 839–850.

Poorter, H., O. Knopf, I. J. Wright, A. A. Temme, S. W. Hogewoning, A. Graf, L. A. Cernusak, and T. L. Pons (2022). A meta-analysis of responses of C_3 plants to atmospheric CO_2: dose–response curves for 85 traits ranging from

the molecular to the whole-plant level. *New Phytologist 233*(4), 1560–1596.

Prentice, I. C., N. Dong, S. M. Gleason, V. Maire, and I. J. Wright (2014). Balancing the costs of carbon gain and water transport: testing a new theoretical framework for plant functional ecology. *Ecology Letters 17*(1), 82–91.

Prentice, I. C., X. Liang, B. E. Medlyn, and Y.-P. Wang (2015). Reliable, robust and realistic: The three R's of next-generation land-surface modelling. *Atmospheric Chemistry and Physics 15*, 5987–6005.

Querejeta, J. I., I. Prieto, C. Armas, F. Casanoves, J. S. Diémé, M. Diouf, H. Yossi, B. Kaya, F. I. Pugnaire, and G. M. Rusch (2022). Higher leaf nitrogen content is linked to tighter stomatal regulation of transpiration and more efficient water use across dryland trees. *New Phytologist 235*(4), 1351–1364.

R Core Team (2021). R: A language and environment for statistical computing.

Raich, J. W., D. A. Clark, L. Schwendenmann, and T. E. Wood (2014). Aboveground tree growth varies with belowground carbon allocation in a tropical rainforest environment. *PLoS ONE 9*(6), e100275.

Rastetter, E. B., P. M. Vitousek, C. B. Field, G. R. Shaver, D. Herbert, and G. I. Ågren (2001). Resource optimization and symbiotic nitrogen fixation. *Ecosystems 4*(4), 369–388.

Reich, P. B. (2014). The world-wide 'fast-slow' plant economics spectrum: a traits manifesto. *Journal of Ecology 102*(2), 275–301.

Reich, P. B., S. E. Hobbie, T. Lee, D. S. Ellsworth, J. B. West, D. Tilman, J. M. H. Knops, S. Naeem, and J. Trost (2006). Nitrogen limitation con-

strains sustainability of ecosystem response to CO₂. *Nature 440*(7086), 922–925.

Rhine, E. D., R. L. Mulvaney, E. J. Pratt, and G. K. Sims (1998). Improving the Berthelot reaction for determining ammonium in soil extracts and water. *Soil Science Society of America Journal 62*(2), 473.

Rogers, A. (2014). The use and misuse of V_{cmax} in Earth System Models. *Photosynthesis Research 119*(1-2), 15–29.

Rogers, A., B. E. Medlyn, J. S. Dukes, G. B. Bonan, S. Caemmerer, M. C. Dietze, J. Kattge, A. D. B. Leakey, L. M. Mercado, Ü. Niinemets, I. C. Prentice, S. P. Serbin, S. Sitch, D. A. Way, and S. Zaehle (2017). A roadmap for improving the representation of photosynthesis in Earth system models. *New Phytologist 213*(1), 22–42.

Saathoff, A. J. and J. Welles (2021). Gas exchange measurements in the unsteady state. *Plant Cell and Environment 44*(11), 3509–3523.

Saleh, A. M., M. Abdel-Mawgoud, A. R. Hassan, T. H. Habeeb, R. S. Yehia, and H. AbdElgawad (2020). Global metabolic changes induced by arbuscular mycorrhizal fungi in oregano plants grown under ambient and elevated levels of atmospheric CO_2. *Plant Physiology and Biochemistry 151*, 255–263.

Schaefer, K., C. R. Schwalm, C. Williams, M. A. Arain, A. Barr, J. M. Chen, K. J. Davis, D. Dimitrov, T. W. Hilton, D. Y. Hollinger, E. Humphreys, B. Poulter, B. M. Raczka, A. D. Richardson, A. Sahoo, P. Thornton, R. Vargas, H. Verbeeck, R. Anderson, I. Baker, T. A. Black, P. Bolstad, J. Chen, P. S. Curtis, A. R. Desai, M. C. Dietze, D. Dragoni, C. M. Gough, R. F. Grant, L. Gu, A. K. Jain, C. Kucharik, B. E. Law, S. Liu, E. Lokipitiya,

H. A. Margolis, R. Matamala, J. H. McCaughey, R. Monson, J. W. Munger, W. Oechel, C. Peng, D. T. Price, D. Ricciuto, W. J. Riley, N. Roulet, H. Tian, C. Tonitto, M. Torn, E. Weng, and X. Zhou (2012). A model-data comparison of gross primary productivity: Results from the North American Carbon Program site synthesis. *Journal of Geophysical Research: Biogeosciences 117*(G3), G03010.

Schneider, C. A., W. S. Rasband, and K. W. Eliceiri (2012). NIH Image to ImageJ: 25 years of image analysis. *Nature Methods 9*(7), 671–675.

Scott, H. G. and N. G. Smith (2022). A Model of C4 Photosynthetic Acclimation Based on Least-Cost Optimality Theory Suitable for Earth System Model Incorporation. *Journal of Advances in Modeling Earth Systems 14*(3), 1–16.

Shi, M., J. B. Fisher, E. R. Brzostek, and R. P. Phillips (2016). Carbon cost of plant nitrogen acquisition: Global carbon cycle impact from an improved plant nitrogen cycle in the Community Land Model. *Global Change Biology 22*(3), 1299–1314.

Shi, M., J. B. Fisher, R. P. Phillips, and E. R. Brzostek (2019). Neglecting plant–microbe symbioses leads to underestimation of modeled climate impacts. *Biogeosciences 16*(2), 457–465.

Smith, N. G. and J. S. Dukes (2013). Plant respiration and photosynthesis in global-scale models: incorporating acclimation to temperature and CO 2. *Global Change Biology 19*(1), 45–63.

Smith, N. G. and T. F. Keenan (2020). Mechanisms underlying leaf photosynthetic acclimation to warming and elevated CO2 as inferred from least-cost optimality theory. *Global Change Biology 26*(9), 5202–5216.

Smith, N. G., T. F. Keenan, I. C. Prentice, H. Wang, I. J. Wright, Ü. Niinemets, K. Y. Crous, T. F. Domingues, R. Guerrieri, F. oko Ishida, J. Kattge, E. L. Kruger, V. Maire, A. Rogers, S. P. Serbin, L. Tarvainen, H. F. Togashi, P. A. Townsend, M. Wang, L. K. Weerasinghe, and S.-X. Zhou (2019). Global photosynthetic capacity is optimized to the environment. *Ecology Letters 22*(3), 506–517.

Smith, N. G., D. L. Lombardozzi, A. Tawfik, G. B. Bonan, and J. S. Dukes (2017). Biophysical consequences of photosynthetic temperature acclimation for climate. *Journal of Advances in Modeling Earth Systems 9*(1), 536–547.

Smith, N. G., S. L. Malyshev, E. Shevliakova, J. Kattge, and J. S. Dukes (2016). Foliar temperature acclimation reduces simulated carbon sensitivity to climate. *Nature Climate Change 6*(4), 407–411.

Smith, S. E. and D. J. Read (2008). *Mycorrhizal Symbiosis*. Academic Press.

Soil Survey Staff (2022). Web Soil Survey. *Natural Resources Conservation Service, United States Department of Agriculture, Available online at the following link: http://websoilsurvey.sc.egov.usda.gov/. Accessed 11/18/2022*.

Soudzilovskaia, N. A., J. C. Douma, A. A. Akhmetzhanova, P. M. van Bodegom, W. K. Cornwell, E. J. Moens, K. K. Treseder, and J. H. C. Cornelissen (2015). Global patterns of plant root colonization intensity by mycorrhizal fungi explained by climate and soil chemistry. *Global Ecology and Biogeography 24*(3), 371–382.

Sulman, B. N., E. Shevliakova, E. R. Brzostek, S. N. Kivlin, S. L. Malyshev, D. N. L. Menge, and X. Zhang (2019). Diverse mycorrhizal associations enhance terrestrial C storage in a global model. *Global Biogeochemical Cy-*

cles 33(4), 501–523.

Sweet, S. K., D. W. Wolfe, A. DeGaetano, and R. Benner (2017). Anatomy of the 2016 drought in the Northeastern United States: Implications for agriculture and water resources in humid climates. *Agricultural and Forest Meteorology 247*, 571–581.

Taylor, B. N. and D. N. L. Menge (2018). Light regulates tropical symbiotic nitrogen fixation more strongly than soil nitrogen. *Nature Plants 4*(9), 655–661.

Terrer, C., S. Vicca, B. A. Hungate, R. P. Phillips, and I. C. Prentice (2016). Mycorrhizal association as a primary control of the CO_2 fertilization effect. *Science 353*(6294), 72–74.

Terrer, C., S. Vicca, B. D. Stocker, B. A. Hungate, R. P. Phillips, P. B. Reich, A. C. Finzi, and I. C. Prentice (2018). Ecosystem responses to elevated CO_2 governed by plant–soil interactions and the cost of nitrogen acquisition. *New Phytologist 217*(2), 507–522.

Thomas, R. Q., E. N. J. Brookshire, and S. Gerber (2015). Nitrogen limitation on land: how can it occur in Earth system models? *Global Change Biology 21*(5), 1777–1793.

Thomas, R. Q., S. Zaehle, P. H. Templer, and C. L. Goodale (2013). Global patterns of nitrogen limitation: confronting two global biogeochemical models with observations. *Global Change Biology 19*(10), 2986–2998.

Thornton, P. E., J.-F. Lamarque, N. A. Rosenbloom, and N. M. Mahowald (2007). Influence of carbon-nitrogen cycle coupling on land model response

to CO₂ fertilization and climate variability. *Global Biogeochemical Cycles 21*(4), GB4018.

Tingey, D. T., D. L. Phillips, and M. G. Johnson (2000). Elevated CO_2 and conifer roots: effects on growth, life span and turnover. *New Phytologist 147*(1), 87–103.

Udvardi, M. and P. S. Poole (2013). Transport and metabolism in legume-rhizobia symbioses. *Annual Review of Plant Biology 64*, 781–805.

Uselman, S. M., R. G. Qualls, and R. B. Thomas (2000). Effects of increased atmospheric CO_2, temperature, and soil N availability on root exudation of dissolved organic carbon by a N-fixing tree (*Robinia pseudoacacia* L.). *Plant and Soil 222*, 191–202.

van Diepen, L. T. A., E. A. Lilleskov, K. S. Pregitzer, and R. M. Miller (2007). Decline of arbuscular mycorrhizal fungi in northern hardwood forests exposed to chronic nitrogen additions. *New Phytologist 176*(1), 175–183.

Vance, C. P. and G. H. Heichel (1991). Carbon in N_2 fixation: Limitation or exquisite adaptation. *Annual Review of Plant Physiology and Plant Molecular Biology 42*(1), 373–392.

Viet, H. D., J.-H. Kwak, K.-S. Lee, S.-S. Lim, M. Matsushima, S. X. Chang, K.-H. Lee, and W.-J. Choi (2013). Foliar chemistry and tree ring $\delta^{13}C$ of *Pinus densiflora* in relation to tree growth along a soil pH gradient. *Plant and Soil 363*(1-2), 101–112.

Vitousek, P. M., K. Cassman, C. C. Cleveland, T. Crews, C. B. Field, N. B. Grimm, R. W. Howarth, R. Marino, L. Martinelli, E. B. Rastetter, and

J. I. Sprent (2002). Towards an ecological understanding of biological nitrogen fixation. In *The Nitrogen Cycle at Regional to Global Scales*, pp. 1–45. Springer Netherlands.

Vitousek, P. M. and R. W. Howarth (1991). Nitrogen limitation on land and in the sea: How can it occur? *Biogeochemistry 13*(2), 87–115.

Vitousek, P. M., S. Porder, B. Z. Houlton, and O. A. Chadwick (2010). Terrestrial phosphorus limitation: mechanisms, implications, and nitrogen–phosphorus interactions. *Ecological Applications 20*(1), 5–15.

Walker, A. P., A. P. Beckerman, L. Gu, J. Kattge, L. A. Cernusak, T. F. Domingues, J. C. Scales, G. Wohlfahrt, S. D. Wullschleger, and F. I. Woodward (2014). The relationship of leaf photosynthetic traits - V_{cmax} and J_{max} - to leaf nitrogen, leaf phosphorus, and specific leaf area: a meta-analysis and modeling study. *Ecology and Evolution 4*(16), 3218–3235.

Wang, H., I. C. Prentice, T. F. Keenan, T. W. Davis, I. J. Wright, W. K. Cornwell, B. J. Evans, and C. Peng (2017). Towards a universal model for carbon dioxide uptake by plants. *Nature Plants 3*(9), 734–741.

Wang, W., Y. Wang, G. Hoch, Z. Wang, and J. Gu (2018). Linkage of root morphology to anatomy with increasing nitrogen availability in six temperate tree species. *Plant and Soil 425*(1-2), 189–200.

Weatherburn, M. W. (1967). Phenol-hypochlorite reaction for determination of ammonia. *Analytical Chemistry 39*(8), 971–974.

Wellburn, A. R. (1994). The spectral determination of chlorophylls a and b, as well as total carotenoids, using various solvents with spectrophotometers of

different resolution. *Journal of Plant Physiology 144*(3), 307–313.

Wen, Z., P. J. White, J. Shen, and H. Lambers (2022). Linking root exudation to belowground economic traits for resource acquisition. *New Phytologist 233*(4), 1620–1635.

Westerband, A. C., I. J. Wright, V. Maire, J. Paillassa, I. C. Prentice, O. K. Atkin, K. J. Bloomfield, L. A. Cernusak, N. Dong, S. M. Gleason, C. Guilherme Pereira, H. Lambers, M. R. Leishman, Y. Malhi, and R. H. Nolan (2023). Coordination of photosynthetic traits across soil and climate gradients. *Global Change Biology 29*(3), 1–29.

Wieder, W. R., C. C. Cleveland, W. K. Smith, and K. Todd-Brown (2015). Future productivity and carbon storage limited by terrestrial nutrient availability. *Nature Geoscience 8*(6), 441–444.

Wieder, W. R., D. M. Lawrence, R. A. Fisher, G. B. Bonan, S. J. Cheng, C. L. Goodale, A. S. Grandy, C. D. Koven, D. L. Lombardozzi, K. W. Oleson, and R. Q. Thomas (2019). Beyond static benchmarking: using experimental manipulations to evaluate land model assumptions. *Global Biogeochemical Cycles 33*(10), 1289–1309.

Wright, I. J., P. B. Reich, and M. Westoby (2003). Least-cost input mixtures of water and nitrogen for photosynthesis. *The American Naturalist 161*(1), 98–111.

Wright, I. J., P. B. Reich, M. Westoby, D. D. Ackerly, Z. Baruch, F. Bongers, J. Cavender-Bares, T. Chapin, J. H. C. Cornelissen, M. Diemer, J. Flexas, E. Garnier, P. K. Groom, J. Gulias, K. Hikosaka, B. B. Lamont, T. Lee, W. Lee, C. Lusk, J. J. Midgley, M.-L. Navas, Ü. Niinemets, J. Oleksyn,

N. Osada, H. Poorter, P. Poot, L. Prior, V. I. Pyankov, C. Roumet, S. C. Thomas, M. G. Tjoelker, E. J. Veneklaas, and R. Villar (2004). The worldwide leaf economics spectrum. *Nature 428*(6985), 821–827.

Xu-Ri and I. C. Prentice (2017). Modelling the demand for new nitrogen fixation by terrestrial ecosystems. *Biogeosciences 14*(7), 2003–2017.

Zaehle, S., B. E. Medlyn, M. G. De Kauwe, A. P. Walker, M. C. Dietze, T. Hickler, Y. Luo, Y. P. Wang, B. El-Masri, P. Thornton, A. Jain, S. Wang, D. Warlind, E. Weng, W. Parton, C. M. Iversen, A. Gallet-Budynek, H. Mccarthy, A. C. Finzi, P. J. Hanson, I. C. Prentice, R. Oren, and R. J. Norby (2014). Evaluation of 11 terrestrial carbon-nitrogen cycle models against observations from two temperate Free-Air CO_2 Enrichment studies. *New Phytologist 202*(3), 803–822.

Zaehle, S., S. Sitch, B. Smith, and F. Hatterman (2005). Effects of parameter uncertainties on the modeling of terrestrial biosphere dynamics. *Global Biogeochemical Cycles 19*(3), GB3020.

Zhu, Q., W. J. Riley, J. Tang, N. Collier, F. M. Hoffman, X. Yang, and G. Bisht (2019). Representing nitrogen, phosphorus, and carbon interactions in the E3SM land model: development and global benchmarking. *Journal of Advances in Modeling Earth Systems 11*(7), 2238–2258.

Ziegler, C., M. E. Dusenge, B. Nyirambangutse, E. Zibera, G. Wallin, and J. Uddling (2020). Contrasting Dependencies of Photosynthetic Capacity on Leaf Nitrogen in Early- and Late-Successional Tropical Montane Tree Species. *Frontiers in Plant Science 11*, 1–12.

Ziehn, T., J. Kattge, W. Knorr, and M. Scholze (2011). Improving the pre-

dictability of global CO2 assimilation rates under climate change. *Geophysical Research Letters 38*(10), L10404.